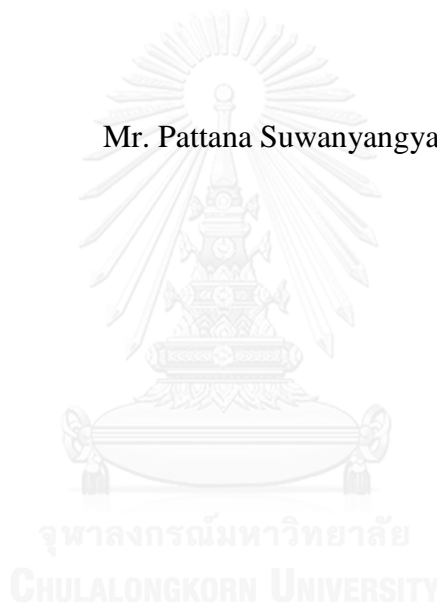


MORPHOLOGICAL EVOLUTION, GROWTH MECHANISM AND  
STRUCTURAL PHASE TRANSFORMATION  
OF ELO GaN NANOSTRUCTURES ON GaAs (001)

Mr. Pattana Suwanyangyaun



บทคัดย่อและแฟ้มข้อมูลฉบับเต็มของวิทยานิพนธ์ตั้งแต่ปีการศึกษา 2554 ที่ให้บริการในคลังปัญญาจุฬาฯ (CUIR)  
เป็นแฟ้มข้อมูลของนิสิตเจ้าของวิทยานิพนธ์ ที่ส่งผ่านทางบัณฑิตวิทยาลัย

The abstract and full text of theses from the academic year 2011 in Chulalongkorn University Intellectual Repository (CUIR)  
are the thesis authors' files submitted through the University Graduate School.

A Dissertation Submitted in Partial Fulfillment of the Requirements  
for the Degree of Doctor of Philosophy Program in Nanoscience and Technology  
(Interdisciplinary Program)  
Graduate School  
Chulalongkorn University  
Academic Year 2015  
Copyright of Chulalongkorn University

วิทยานิพนธ์การเชิงสัณฐาน กลไกการปลูกผลึกและการเปลี่ยนเฟสเชิงโครงสร้างของโครงสร้าง  
นาโน GaN อีแอลโอ บน GaAs (001)



วิทยานิพนธ์นี้เป็นส่วนหนึ่งของการศึกษาตามหลักสูตรปริญญาวิทยาศาสตรดุษฎีบัณฑิต

สาขาวิชาวิทยาศาสตร์นาโนและเทคโนโลยี (สหสาขาวิชา)

บัณฑิตวิทยาลัย จุฬาลงกรณ์มหาวิทยาลัย

ปีการศึกษา 2558

ลิขสิทธิ์ของจุฬาลงกรณ์มหาวิทยาลัย

Thesis Title MORPHOLOGICAL EVOLUTION, GROWTH  
MECHANISM AND STRUCTURAL PHASE  
TRANSFORMATION OF ELO GaN  
NANOSTRUCTURES ON GaAs (001)

By Mr. Pattana Suwanyangyaun

Field of Study Nanoscience and Technology

Thesis Advisor Assistant Professor Sakuntam Sanorpim, Ph.D.

Thesis Co-Advisor Chanchana Thanachayanont, Ph.D.

---

Accepted by the Graduate School, Chulalongkorn University in Partial  
Fulfillment of the Requirements for the Doctoral Degree

..... Dean of the Graduate School  
(Associate Professor Sunait Chutintaranond, Ph.D.)

#### THESIS COMMITTEE

..... Chairman  
(Associate Professor Vudhichai Parasuk, Ph.D.)

..... Thesis Advisor  
(Assistant Professor Sakuntam Sanorpim, Ph.D.)

..... Thesis Co-Advisor  
(Chanchana Thanachayanont, Ph.D.)

..... Examiner  
(Assistant Professor Sukkaneste Tungasmita, Ph.D.)

..... Examiner  
(Ratthapol Rangkupan, Ph.D.)

..... External Examiner  
(Somyod Denchitcharoen, Ph.D.)



# # 5487843920 : MAJOR NANOSCIENCE AND TECHNOLOGY

KEYWORDS: GALLIUM NITRIDE / CRYSTAL STRUCTURE / RAMAN SPECTROSCOPY / HIGH RESOLUTION X-RAY DIFFRACTION / METALORGANIC VAPOR PHASE EPITAXY

PATTANA SUWANYANGYAUN: MORPHOLOGICAL EVOLUTION, GROWTH MECHANISM AND STRUCTURAL PHASE TRANSFORMATION OF ELO GaN NANOSTRUCTURES ON GaAs (001). ADVISOR: ASST. PROF. SAKUNTAM SANORPIM, Ph.D., CO-ADVISOR: CHANCHANA THANACHAYANONT, Ph.D., 77 pp.

Epitaxial lateral overgrown (ELO) cubic-phase gallium nitride (c-GaN) films with a selective area growth method were grown on the [100], [1-10] and [110] mask-stripe patterned GaAs (001) substrates by metalorganic vapor phase epitaxy. The growth morphologies of ELO c-GaN films for each mask-stripe direction were investigated by scanning electron microscope (SEM). The results show that c-GaN films on [100] mask stripe pattern exhibited unidentified sidewall facets, on [1-10] mask stripe pattern demonstrated the dominant (113) side wall facets and, finally, on [1-10] mask stripe pattern revealed dominant (111) sidewall facets. Confocal Raman microscope was an instrument to investigate crystal structure that cubic or hexagonal phases on top and sidewall facet of c-GaN films in the specific area of 2  $\mu\text{m}$  in diameter. The structural phase transformation in the ELO c-GaN films was study by varying growth time. High resolution X-ray diffraction analysis was performed to investigate crystal structures and crystal quality of the ELO c-GaN films for each mask stripe direction. Hexagonal phase inclusion was calculated from the integrated X-ray intensities ratio between c-GaN (002) and h-GaN (10-11) reflections extracted from the reciprocal space mappings. Based on our results, normally cubic phase structure has dominant on the (113) sidewall facets and hexagonal phase structure has dominant on the (111) sidewall facets. However, the growth time is not the only parameter that effects on structural phase transformation. Selective area growth with controlled mask fill-factor (FF) is another important parameter to control structural phase transformation. With the suitable mask fill factor ( $\text{FF} > 0.7$ ), ELO c-GaN for the [110] mask stripe direction on GaAs (001) showed a good crystal quality and very high cubic phase quantity.

Field of Study: Nanoscience and Technology

Academic Year: 2015

Student's Signature .....

Advisor's Signature .....

Co-Advisor's Signature .....

## ACKNOWLEDGEMENTS

This dissertation cannot be completed without their opinions. First and foremost, I would like to express my deepest gratitude to my advisor, Assistant Professor Dr. Sakuntam Sanorpim. Without him, I will not have the opportunity to complete a doctoral degree. He guides me along the right paths when I have problems. My co-advisor, Dr. Chanchana Thanachayanont, who give me some advices.

I am grateful to my thesis committee Associate Professor Dr. Vudhichai Parasuk, Assistant Professor Dr. Sukkaneste Tungasmita, Dr. Ratthapol Rangkupan and Dr. Somyod Denchitcharoen for making the valuable suggestions and comments to improve this dissertation.

Special thanks goes to Mrs. Nasuangorn Yopanaksakdi who is a Program Coordinator in Nanoscience and Technology for helping me preparing the academic and financial documents.

I would like to thank my colleagues from AMPRG members. Especially, Mrs. Pawinee Klangtakai, Ms. Dares Kaewket, Ms. Jamreonta Parinyataramas, Ms. Papaporn Jantawongrit, Mrs. Pornsiri Wanarattikan, Mr. Phongbandhu Sirirattanawong, Mr. Pitsaya Praigaew, Mr. Noppadon Toongyai, Mr. Kunpot Mopoung, Ms. Nattamon Suwannahan, Mr. Nutthapong Discharoen and Mr. Taworn Intaro. Without their support, this research would not have been completed.

I would like to acknowledge the financial support from Center of Innovative Nanotechnology (CIN) under management of Chulalongkorn University for tuition fees (3 years), The 90th anniversary of Chulalongkorn university fund (Ratchadaphiseksomphot Endowment Fund), The Ratchadaphiseksomphot Endowment Fund of Chulalongkorn University (RES560530227-AM) and Conference grant for Ph.D. Student.

Last but not the least, I would like to express my appreciation to my parents who love, understand and encourage me. I also express my appreciation to Ms. Chanutr Chinratanapisit, for all her love and support.

## CONTENTS

	Page
THAI ABSTRACT .....	iv
ENGLISH ABSTRACT.....	v
ACKNOWLEDGEMENTS .....	vi
CONTENTS.....	vii
LIST OF FIGURES .....	x
LIST OF TABLES .....	xiv
CHAPTER I.....	1
INTRODUCTION .....	1
1.1 Overview of Gallium Nitride (History and Motivation).....	1
1.2 Objectives and Scope.....	7
1.3 Expectations.....	7
1.4 Organizations of the Dissertation .....	8
CHAPTER II.....	9
ELO CUBIC GaN.....	9
2.1 GaAs Substrate .....	9
2.2 Buffer Layer.....	14
2.3 Selective Area Growth (SAG).....	16
2.3.1 Dot Pattern.....	17
2.3.2 Line Pattern .....	18
2.4 Epitaxial Lateral Overgrowth (ELO).....	18
2.5 Mask Fill Factor.....	19
2.6 Growth Temperature.....	21
CHAPTER III .....	23
GROWTH PROCESS AND CHARACTERIZATION .....	23
3.1 MOVPE Growth Process .....	23
3.1.1 Mask Stripe Directions .....	23
3.1.2 ELO c-GaN Film Growth Process.....	24
3.1.3 Sample Structure .....	26

	Page
3.2 Characterization Techniques.....	27
3.2.1 Scanning Electron Microscope (SEM).....	28
3.2.2 Micro-Raman Scattering .....	29
3.2.3 High Resolution X-ray Diffraction (HRXRD).....	32
3.2.3.1 $2\theta/\omega$ -scan mode .....	34
3.2.3.2 Rocking curve ( $\omega$ -scan) mode .....	34
3.2.3.3 Reciprocal space mapping (RSM) mode.....	35
CHAPTER IV .....	40
EXPERIMENTAL RESULTS.....	40
4.1 Optical Image.....	40
4.2 Scanning Electron Microscopy (SEM).....	43
4.2.1 Plane View of SEM Images .....	44
4.2.2 Cross-sectional View of SEM Images.....	45
4.3 Micro Raman Scattering Spectroscopy .....	48
4.4 High Resolution X-ray Diffraction .....	52
4.4.1 $2\theta/\omega$ -scan Profiles .....	52
4.4.2 Rocking Curve.....	54
4.4.3 Reciprocal Space Mapping.....	57
CHAPTER V .....	64
CONCLUSIONS.....	64
REFERENCES .....	66
APPENDIX.....	71
APPENDIX A.....	72
LIST OF ACRONYMS .....	72
APPENDIX B .....	74
LIST OF PUBLICATION AND CONFERENCES .....	74
VITA.....	77

## LIST OF FIGURES

Figure 1.1: Band gap energy of hexagonal or wurtzite ( $\alpha$ -phase) and cubic or zincblende ( $\beta$ -phase) structures .....	1
Figure 1.2: Visible light wavelength from violet 380 nm to red 740 nm and RGB color model .....	2
Figure 1.3: Crystal structure of hexagonal (wurtzite) GaN and cubic (zincblende) GaN.....	4
Figure 1.4: Potential profile of hexagonal GaN/AlGaN quantum well structures. (a) polar c-plane and (b) non-polar plane .....	5
Figure 1.5: Lattice mismatch of c-GaN with other substrates and thermal expansion coefficient (TEC).....	6
Figure 2.1: Misfit dislocation and threading dislocation lines in layer. ....	10
Figure 2.2: Top and side views of h-GaN [0001] and c-GaN [111].....	11
Figure 2.3: Planar defect along to [110] cross-section (a) c-GaN on [001], (b) h-GaN on [0001] and (c) stacking fault and twin defect for c-GaN structure .....	12
Figure 2.4: Cross-sectional SEM images of c-GaN on (a) GaAs (001) and (b) GaAs (311)A.....	14
Figure 2.5: Cross-sectional SEM images of c-GaN on GaAs (100) (a) without and (b) with LT-GaN buffer layer .....	15
Figure 2.6: Top and side view of SAG c-GaN with a) dot and b) line patterns (green color - mask and orange color - windows or open width area). ....	16
Figure 2.7: Schematic diagram of reduction mechanism of SFs during ELO of cubic GaN .....	17
Figure 2.8: Morphologies of SAG c-GaN films along to the [100], [1-10] and [110] mask stripe directions.....	18
Figure 2.9: Growth models of ELO c-GaN on (a) [1-10] and (b) [110] mask pattern GaAs (001).....	19

Figure 2.10: Mask fill factor [M – mask area and W - windows or open width area].....	20
Figure 2.11: Dependence of the hexagonal phase inclusion on the fill factor.....	20
Figure 2.12: Growth features of SAG c-GaN on (a) [011] and (b) [001]-stripe pattern for different growth temperature.....	22
Figure 3.1: Mask pattern along [100], [1-10] and [110] directions on GaAs (001) substrate (green color - mask oxide and grey color - windows area) .....	23
Figure 3.2: The horizontal reactor of MOVPE system .....	24
Figure 3.3: Growth temperature and growth time process of ELO c-GaN with double buffer layers .....	25
Figure 3.4: Sample structure of c-GaN on GaAs (001) with mask stripe pattern and double buffer layers of LT-GaN and GaAs.....	27
Figure 3.5: (a) Signal of incident electron beam to sample and (b) secondary electrons on different surface on sample .....	28
Figure 3.6: Energy diagram of Rayleigh scattering, Stokes and anti-Stokes Raman scattering.....	29
Figure 3.7: (a) Illustrated of HRXRD and (b) photo of Bruker-AXS Discover D8 in High resolution mode.....	32
Figure 3.8: X-ray with Bragg's law .....	33
Figure 3.9: Rocking curve mode ( $\omega$ -scan) of c-GaN (002) .....	34
Figure 3.10: Symmetrical RSM mode of c-GaN (002) on GaAs (a) type of defects and (b) hexagonal phase inclusion {10-11}.....	36
Figure 3.11: c-GaN on GaAs (001) with family plane of {111} [1-10] azimuth axes .....	38
Figure 4.1: Multiple optical microscopy images of SAG/ELO c-GaN on GaAs (001) at growth time of 10 min (sample size 11.4 x 9.9 mm).....	40

Figure 4.2: Optical microscope images (500x) of SAG/ELO c-GaN films on (a-d) [100], (e-h) [1-10] and (i-l) [110] mask pattern GaAs (001) at growth time of 10, 30, 60 and 120 min.....	42
Figure 4.3: Plane view SEM images of SAG/ELO c-GaN on (a-d) [100], (e-h) [1-10] and (i-l) [110] mask pattern GaAs (001) at the growth time of 10 to 120 min .....	44
Figure 4.4: Cross-sectional view SEM images of SAG/ELO c-GaN on (a-d) [100], (e-h) [1-10] and (i-l) [110] mask pattern GaAs (001) at the growth time of 10 to 120 min .....	45
Figure 4.5: Cross-sectional view of SEM images (x6000) of ELO c-GaN on GaAs (001) a) [1-10] at growth time of 30 min and b) [110] at growth time of 120 min .....	47
Figure 4.6: Micro Raman spot size $\sim 2 \mu\text{m}$ on the top and side facets of SAG/ELO c-GaN films.....	48
Figure 4.7: Raman spectra on the top area of SAG/ELO c-GaN on [1-10] mask patterned GaAs (001) at growth time of 120 minutes.....	50
Figure 4.8: Raman spectra of ELO c-GaN on GaAs (001) on the top and sidewall facets with different growth times and mask stripe directions .....	51
Figure 4.9: HRXRD $2\theta/\omega$ -scan profiles of SAG/ELO c-GaN on [100], [1-10] and [110] mask stripe patterned GaAs (001) and normalized FWHM $\Delta(2\theta/\omega)$ profiles of c-GaN (002).....	53
Figure 4.10: HRXRD c-GaN (002) $\omega$ -scan profiles of incident X-ray directions perpendicular and parallel with [100], [1-10] and [110] mask stripe directions .....	55
Figure 4.11: $\omega$ -scan profiles of incident X-ray perpendicular and parallel to [100], [1-10] and [110] mask stripe directions at growth time of 10 to 120 min.....	56
Figure 4.12: Symmetrical RSMs of c-GaN (002) for [100] mask stripe pattern with normalized c-GaN (002) individual growth times.....	58
Figure 4.13: Symmetrical RSMs of c-GaN (002) for [1-10] mask stripe pattern with normalized c-GaN (002) individual growth times.....	59

Figure 4.14: Symmetrical RSMs of c-GaN (002) for [110] mask stripe pattern with normalized c-GaN (002) individual growth times.....	60
Figure 4.15: (a) Raman spectra of c-GaN stripe on the top and sidewall facets and (b) Integrated Raman intensities ratio of c-GaN (LO) to c-GaN (LO) with h-GaN $E_2$ high.....	63
Figure 4.16: Morphologies of ELO c-GaN on [110] mask stripe pattern GaAs (001) (a) with h-GaN dominant and (b) with c-GaN dominant.....	63



## LIST OF TABLES

Table 3.1: Phonon modes in cubic and hexagonal GaN .....	30
Table 3.2: Theoretical calculation X-ray intensities of c-GaN (002) and h-GaN (10-11).....	37
Table 4.1: The vertical growth rate of SAG/ELO c-GaN on [100], [1-10] and [110] mask patterned GaAs (001).....	48
Table 4.2: The growth time with the integrated intensities of hexagonal phase inclusion.....	61



# CHAPTER I

## INTRODUCTION

### 1.1 Overview of Gallium Nitride (History and Motivation)

Gallium nitride (GaN) is one of the III-N semiconductor materials along with aluminium nitride (AlN) and indium nitride (InN) which have unique properties to be produced as optoelectronic and high frequency devices. GaN has a wide band gap energy which can be adjusted by alloying with Al and In to AlGaN, InGaN or AlInGaN.

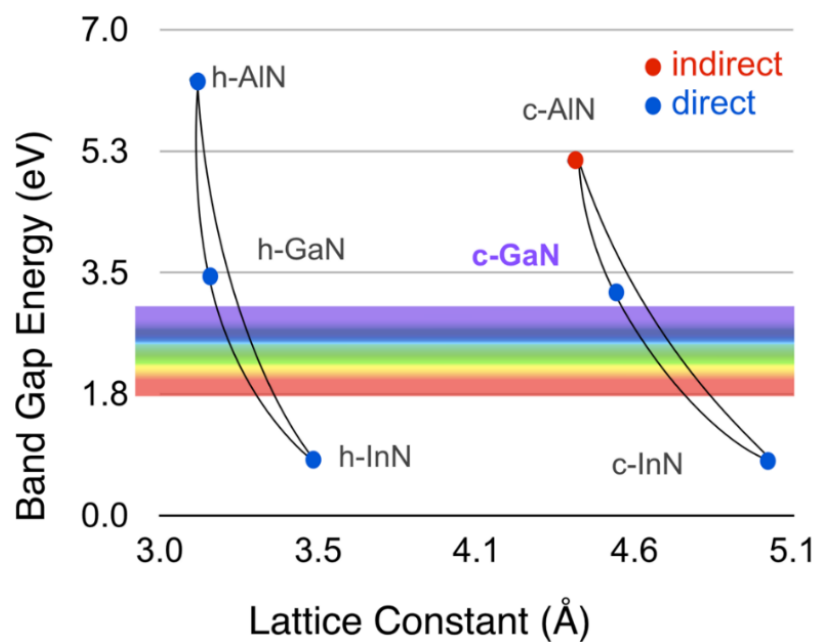


Figure 1.1: Band gap energy of hexagonal or wurtzite ( $\alpha$ -phase) and cubic or zincblende ( $\beta$ -phase) structures [1-3].



Figure 1.2: Visible light wavelength from violet 380 nm to red 740 nm and RGB color model.

The relationship of band gap energy and lattice constant is shown in Fig 1.1 of which the band gap energies of these III-N semiconductor materials cover visible light wavelength region. Al or In doping in GaN can be fabricated to optoelectronics devices such as solar cells, laser diodes (LDs) and light-emitting diodes (LEDs).

For solar cells, the third generation of solar cells is multilayer or tandem cells which call multijunction solar cells. InGaN/GaN multiple-quantum well (MQW) structure as absorber layer of tandem cells can result in high conversion efficiency by 51% with nanorod and nanohole [4]. High power violet and blue LDs are constructed from InGaN based semiconductor materials which are used as LDs for reading Blu-ray Disc (BD). Pure green LDs based on InGaN is an interesting product which has high operating temperature and high efficiency (over 100mW) compared with other green LDs such as gallium phosphide (GaP), aluminium gallium phosphide (AlGaP) and aluminium gallium indium phosphide (AlGaInP) [5]. However, the most interesting in optoelectronics devices for GaN based semiconductor materials is LEDs especially white light-emitting diodes (WLEDs). There are three main methods to produce WLEDs. The first method is blue, green and red LEDs color mixing which the red-green-blue (RGB) model shown in Fig. 1.2. The second method is using

ultraviolet (UV) LEDs with RGB phosphors and the last method is using blue LEDs with yellow phosphor.

Among of them, blue LEDs with yellow phosphor have the highest conversion efficiency and the longest life time. At the beginning, it was difficult to produce blue LEDs because the p-type GaN could not be fabricated. In 1989, Amano et al. invented p-type GaN with Mg doping by metal organic chemical vapour deposition (MOCVD) with post low-energy electron-beam irradiation (LEEBI) treatment however, their electrical properties were not good enough to fabricate LEDs and LDs [6].

The first high efficiency blue LEDs based on InGaN was invented by Nakamura et al. from Nichia Corporation in 1994 by using p-type GaN doped with Al and Mg [7]. In 2014, the Nobel Prize for Physics was awarded to Shuji Nakamura, Isamu Akasaki and Hiroshi Amano for their development of the efficient blue LEDs which can produce WLEDs for energy saving.

By understanding crystal structures of GaN, high effective optoelectronics devices can be fabricated. There are two main crystal structures of GaN which are hexagonal (wurtzite) or alpha ( $\alpha$ -phase) and cubic (zincblende) or beta ( $\beta$ -phase), as shown in Fig. 1.3. The other structure is rocksalt which occurs only at high pressure. The h-GaN structure is a stable form in nature which can be fabricated more easily than the c-GaN structure.

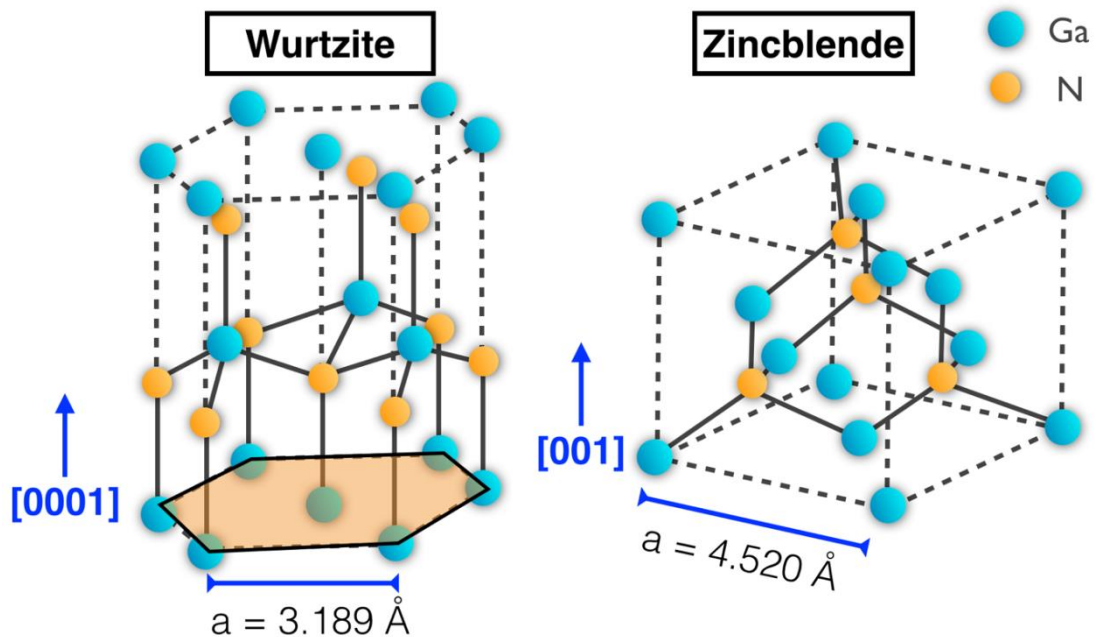


Figure 1.3: Crystal structure of hexagonal (wurtzite) GaN and cubic (zincblende) GaN.

Most of LEDs and LDs based on GaN are constructed from polar c-plane h-GaN (0001). However, the polar c-plane of h-GaN has a disadvantage that it has strong internal electric field from the charge spatial separation within the c-plane h-GaN (0001) based quantum well (QW). This increases effective barrier height leading to a reduced recombination efficiency [8].

The potential profile of polar and non-polar plane GaN/AlGaIn QW shown in Fig. 1.4. The spatial separation between potential band is tilted due to polarization induced internal electric field which makes the wave function at energy level holes in valence band (VB) and energy level of electrons in conduction band (CB) smaller than non-polar plane. This phenomenon is called quantum confined stark effect (QCSE).

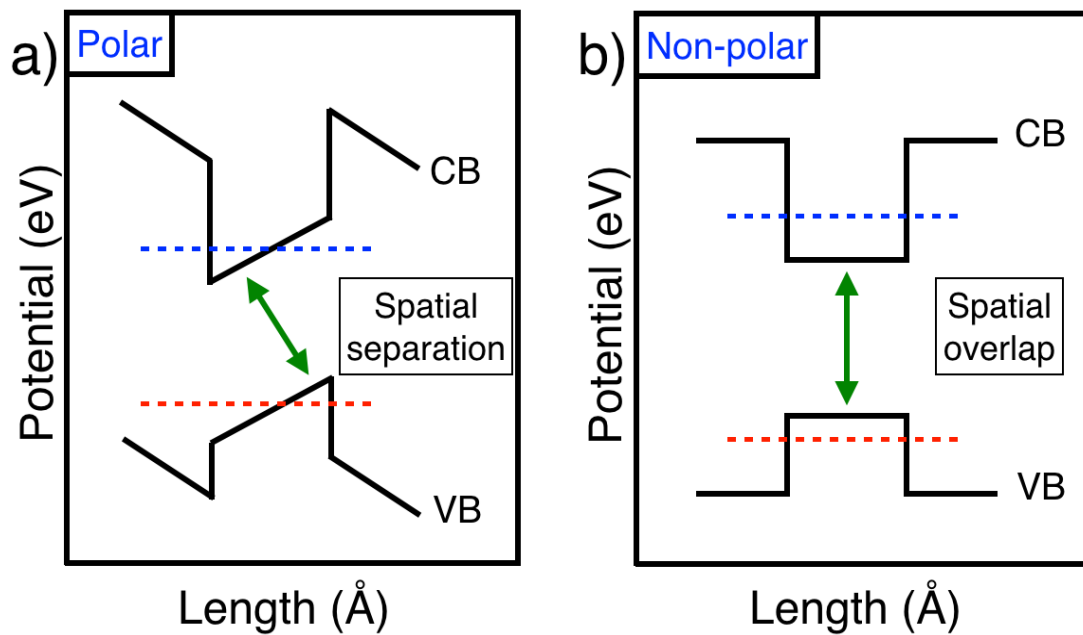


Figure 1.4: Potential profile of hexagonal GaN/AlGaN quantum well structures. (a) polar c-plane and (b) non-polar plane [9].

The band diagram of non-polar plane QW shows wave function that has spatial overlap directly between CB and VB which increases recombination rate.

Non-polar (a-plane or m-plane) or semipolar (r-plane) have been considered to avoid the problem however, those planes are hard to cleave and costly to produce [10, 11]. Another alternative way is using non-polar cubic GaN (c-GaN) (001) because cubic structure has higher crystal symmetry leading to higher electron mobility which is also an advantage for high-speed devices.

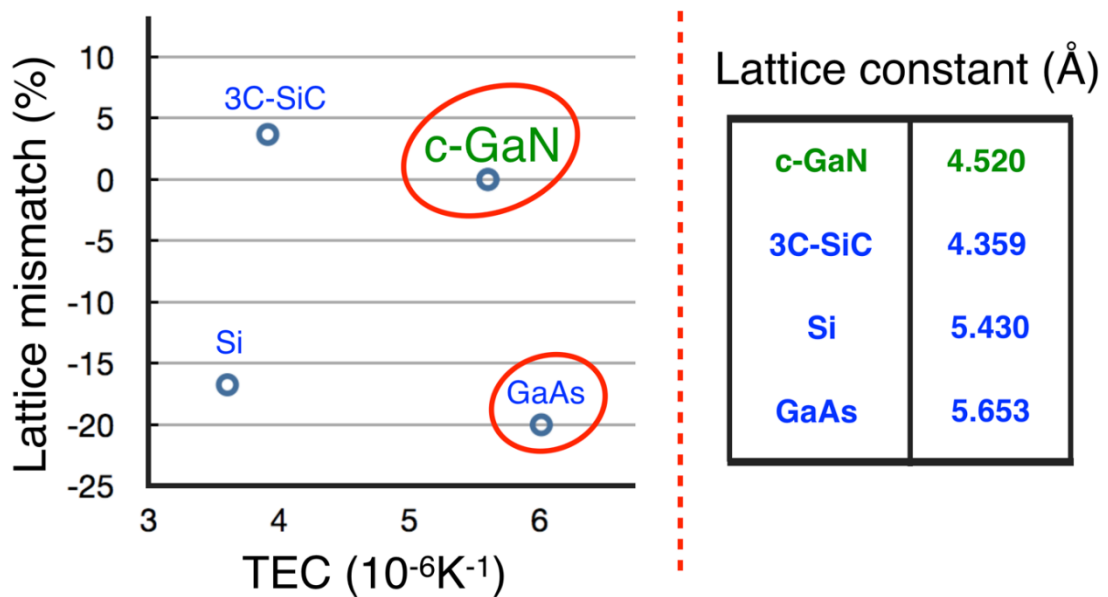


Figure 1.5: Lattice mismatch of c-GaN with other substrates and thermal expansion coefficient (TEC) [12, 13].

However, there are some problems for c-GaN (001) growth such as lack of suitable substrates causing large lattice mismatch between c-GaN film and substrate and c-GaN is an unstable form in nature which is not easy to fabricate.

Gallium arsenide (GaAs) is one promising cubic substrate for growth of c-GaN films because it has thermal expansion coefficient (TEC) near that of c-GaN compared with other cubic substrates such as 3C-SiC (zincblende silicon carbide) and Si (Silicon), see Fig. 1.5. Although a large lattice mismatch will lead to some defects in c-GaN films such as dislocations and stacking faults, severe problems depend on a large TEC mismatch causing residual stress in the c-GaN films which have major impact.

## 1.2 Objectives and Scope

The objectives of this dissertation are as following; (i) to investigate growth morphologies of SAG/ELO cubic GaN with various mask-stripe directions and growth times, (ii) to manipulate the structural phase of GaN using ELO technique and (iii) to verify growth mechanism of SAG/ELO cubic GaN nanostructures.

To complete all objectives, the c-GaN films were grown on [100], [1-10] and [110] mask stripe patterned GaAs (001) by metal organic vapour phase epitaxy (MOVPE). The selective area growth (SAG) and epitaxial lateral overgrowth (ELO) were methods to reduce dislocation density in the films. The growth morphologies of c-GaN films were investigated at growth times of 10 to 120 minutes by scanning electron microscopy (SEM). The nanostructured phase transformation between hexagonal and cubic structures was verified by micro-Raman scattering and high resolution X-ray diffraction (HRXRD) analysis methods. The hexagonal phase inclusion intensities in c-GaN films were confirmed by reciprocal space mapping modes in HRXRD.

## 1.3 Expectations

(i) Understanding growth morphologies in micro- and nano-scales of SAG/ELO cubic GaN films, when mask-stripe directions and growth times were varied.

(ii) Optimizing growth conditions for c-GaN film with low h-GaN content.

## 1.4 Organizations of the Dissertation

This research focuses on characterizations of SAG/ELO c-GaN on GaAs (001) by MOVPE. This dissertation is organized into five parts. In the first chapter, a brief history and introduction of GaN with some applications that GaN has potential to be fabricated as commercial products. The crystal structures of GaN which c-GaN structure is of interest to produce high speed devices. The problem of c-GaN structure is lack of suitable substrates of which among of them GaAs is the most suitable substrate for consideration.

In the **chapter II**, the introduction of defect types is described including the defects that are usually found in c-GaN films such as misfit dislocations, threading dislocations, stacking faults and hexagonal phase inclusion. Some literature reviews SAG and ELO methods to reduce defects and control high cubic phase purity.

The experiment setup for low pressure MOVPE growth system and the growth process to fabricate ELO c-GaN films on [100], [1-10] and [110] mask patterned GaAs (001) are described in **chapter III**. The experimental instruments to use as analysis method which are SEM, micro-Raman spectroscopy and HRXRD will be described with the operation mode for working.

The results from SEM images, micro-Raman scattering on specific area and HRXRD operating modes are described in **chapter IV** with the discussions.

Finally, **chapter V** is conclusion of this dissertation work.

## CHAPTER II

### ELO CUBIC GaN

Because c-GaN is metastable structure in nature, it is really difficult to growth high quality cubic phase GaN films. Many techniques have been used to control the cubic phase GaN with low hexagonal phase inclusion. There are, however, many parameters that can change cubic phase to hexagonal phase GaN. The five major parameters to be considered are substrates, buffer layers, selective area growth with dot or line patterns, mask fill factor and growth temperatures, are considered and described.

#### 2.1 GaAs Substrate

From chapter I, GaAs substrate is chosen among of various cubic structure substrates because the TEC mismatch has the nearest value to c-GaN structure although the lattice mismatch is large ~20%. In epitaxial growth process, there are three types of interfaces between layer and substrate which are coherent, semi-coherent and incoherent interfaces. Coherent interface occurs when layer and substrate have perfect lattice matching such as AlAs on GaAs and InAs on GaAs (001). Semi-coherent interface occurs when layer and substrate have partial lattice matching of which the relative strain is less than 25%. If the relative strain is higher than 25%, it will be an incoherent interface which with no lattice matching at the interface. For c-GaN on GaAs (001), it is the semi-coherent interface which the dislocations appear due to the large lattice mismatch.

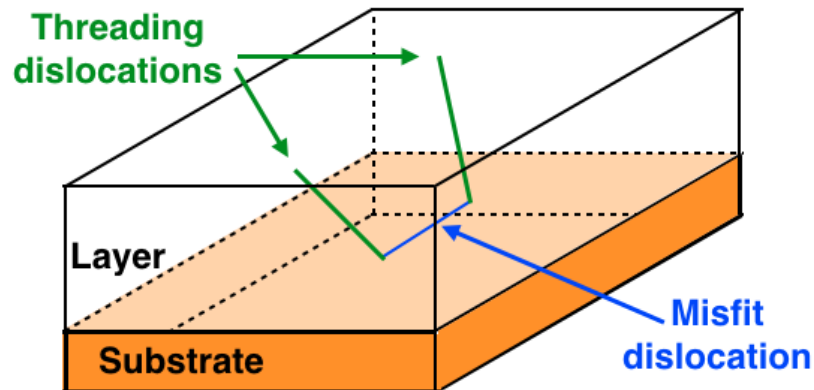


Figure 2.1: Misfit dislocation and threading dislocation lines in layer.

A misfit dislocation occurs by a missing atom in lattice position between layer and substrate which is called the edge dislocation, as shown in Fig. 2.1. Two threading dislocation lines are always generated at the end of one misfit dislocation line. The slip plane is the plane with the highest planar density of atoms which is specific for each crystal structure. In the case of c-GaN structure, the slip plane is  $\{111\}$ . For h-GaN structure slip plane are  $\{0001\}$ ,  $\{10-10\}$  and  $\{10-11\}$ .

Due to the similarity between c-GaN (111) and h-GaN (0001), the planar defects such as stacking fault and twin, are considered. The crystal structures of h-GaN and c-GaN, are shown in Fig. 2.2. The angle of top view between atoms of Ga and N in close-packed planes are 60 degrees for h-GaN structure on  $[0001]$  and 30 degrees for c-GaN structure on  $[111]$ . The yellow planes are referring to the close-packed crystal planes of h-GaN (0001) and c-GaN (111). The side view of both hexagonal and cubic GaN structure look nearly similar.

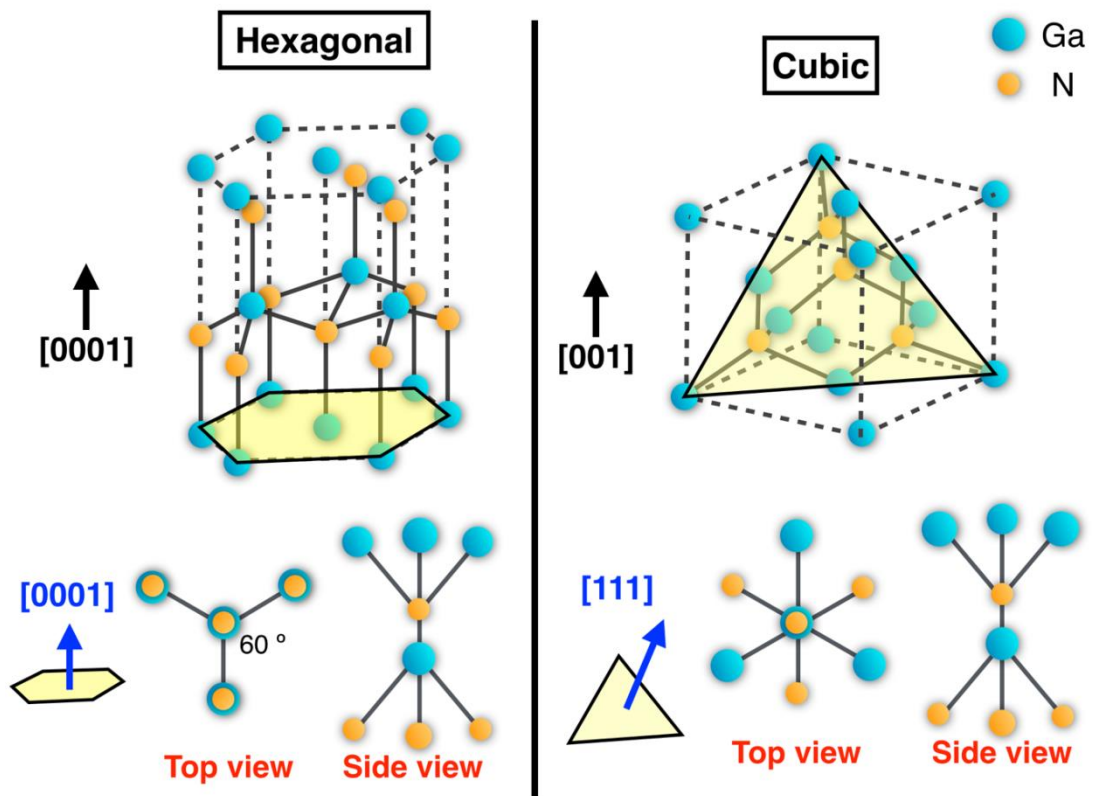


Figure 2.2: Top and side views of h-GaN [0001] and c-GaN [111].

In Fig. 2.3, the planar defects along [110] cross-sectional view is showed how to the stacking fault and twin defect are occurred. The c-GaN structure on [001] with {111} plane is shown in Fig. 2.3 (a) and h-GaN structure on [0001] with {0001} is shown in Fig. 2.3 (b). The stacking fault is occurred at the interface of c-GaN {111} plane and h-GaN {0001} plane while twin defect is occurred from c-GaN {111} plane change to h-GaN {0001} plane and come back to c-GaN with 60 degrees rotated of c-GaN [001] structure, as shown in Fig. 2.3 (c). Normally, stacking faults will have appeared on the interface between c-GaN films and GaAs substrates with certain angle of {111} planar defects at 54.7 degrees.

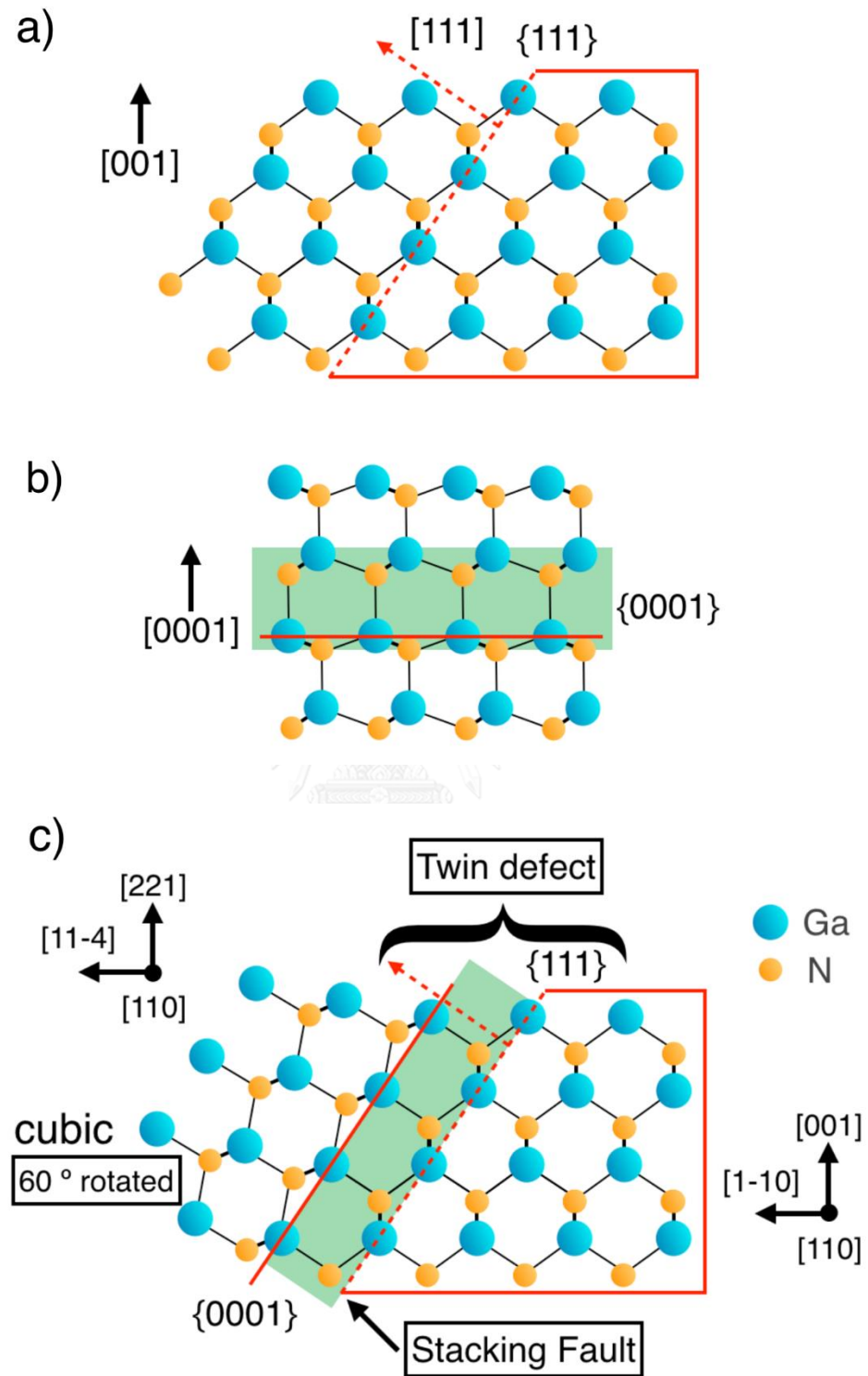


Figure 2.3: Planar defect along to  $[110]$  cross-section (a) c-GaN on  $[001]$ , (b) h-GaN on  $[0001]$  and (c) stacking fault and twin defect for c-GaN structure [14].

To grow c-GaN, there are various directions of GaAs substrates such as GaAs (001), GaAs (111)A, GaAs (111)B or GaAs (311)A. All of them are interesting GaAs substrates to grow high cubic phase purity of c-GaN films. Because SFs always occur at (111) plane, Kuwano et al. [15] reported the formation of c-GaN on GaAs (111)B and investigated by TEM from electron diffraction (ED) patterns. The result showed that SFs propagated along (111) plane and c-GaN was found at the interface of GaAs (111)B because N atoms can diffuse through GaN and GaAs which indicate that c-GaN and GaAs are almost unstrained. Hong et al. [16] reported c-GaN on GaAs (111)A and GaAs (111)B.

Their results from HRTEM images and SAD pattern showed that c-GaN on GaAs (111)A had better interface than GaAs (111)B. The FWHM of XRD for c-GaN on GaAs (111)A and (111)B showed that c-GaN on (111)B GaAs had larger FWHM than (111)A GaAs which resulting more mosaicity in the c-GaN film.

Sanorpim et al. [17] investigated c-GaN on GaAs (311)A. This considered avoiding SFs and structural phase transformation from (111) plane. The c-GaN films were grown on [311] direction. However, the mixing phase of hexagonal GaN was still generated at (111) plane of c-GaN. The result of hexagonal phase inclusion is less than 20% which is comparable to c-GaN on GaAs (001) that leads to c-GaN on GaAs (311)A. Furthermore, c-GaN films on GaAs (311)A also showed smoother interface between c-GaN film and GaAs (311)A substrate while c-GaN films on GaAs (001) substrate has voids area which caused from the thermal decomposition during the growth c-GaN film process, as shown in Fig 2.4.

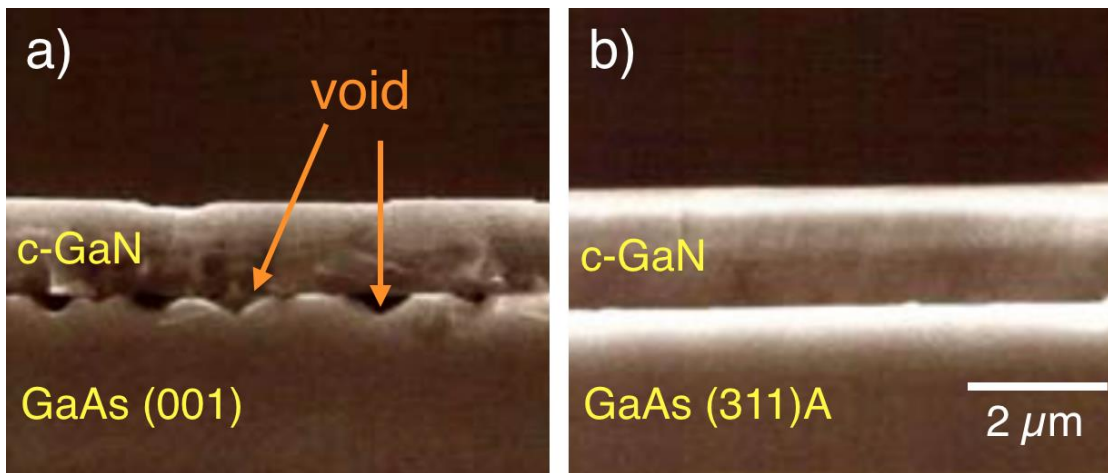


Figure 2.4: Cross-sectional SEM images of c-GaN on (a) GaAs (001) and (b) GaAs (311)A [17].

## 2.2 Buffer Layer

The buffer layer is the important key structure to produce cubic phase GaN. There are many reasons to use a buffer layer to control cubic phase GaN such as reduced lattice mismatch between substrate and film, controlled cubic phase to grow at the interface, prevented thermal decomposition of substrate due to high temperature during the growth process of c-GaN films. The thickness of buffer layer is also important to make to the flat surface of c-GaN films. Cubic phase buffer layer is inserted to control cubic phase GaN films. There are various possible cubic phase buffer layers such as AlAs, AlN, AlGaAs, GaN.

However, AlAs buffer layer with nitridation process produced h-GaN which h-GaN (0001) // GaAs (001). The hexagonal phase GaN was generated at the interface of AlAs where XRD results cannot detect cubic phase GaN. Furthermore, the large lattice mismatch between h-GaN films and AlAs buffer layer cause a large misfit strain [18, 19]. While AlGaAs buffer layer with nitridation can create high c-GaN

films although h-GaN was generated at (111) facet during nitridation process [20]. The AlGaAs buffer layer was grown at 700 °C on GaAs (001) and the growth process of c-GaN can be high at 960 °C without thermal decomposition [21].

As shown in Fig. 2.5, Wu et al. [22] reported that low temperature (LT) GaN buffer layer to protect GaAs substrate from thermal decomposition which the growth process of c-GaN on GaAs (100) can operate at high growth temperature as 980 °C. LT-GaN buffer layer could improve crystal quality of c-GaN film which with FWHM of XRD compared to without buffer layer [16]. Shen et al. [23] reported that the thinner GaN buffer layer had the lower hexagonal phase inclusion in c-GaN films.

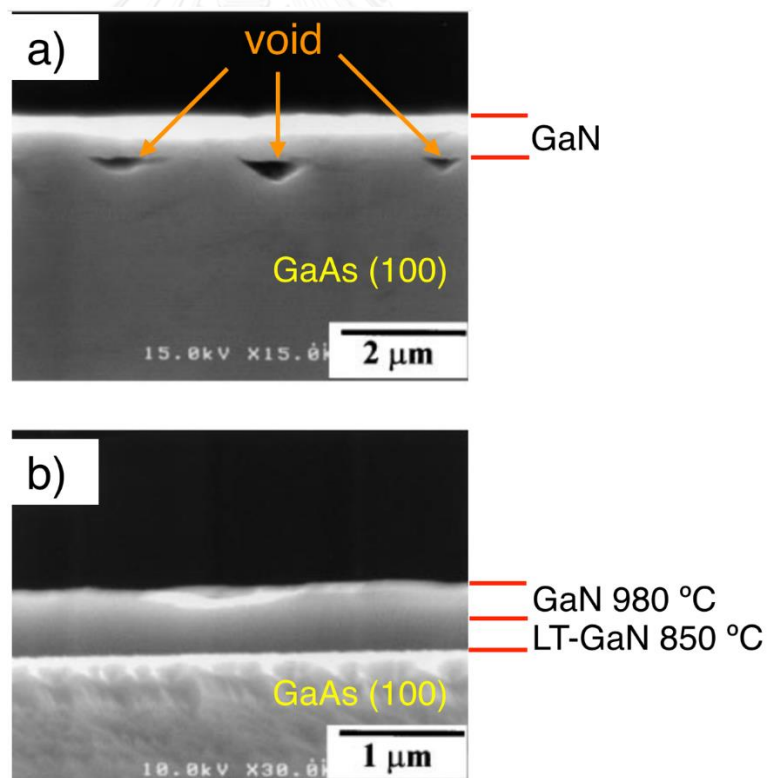


Figure 2.5: Cross-sectional SEM images of c-GaN on GaAs (100) (a) without and (b) with LT-GaN buffer layer [22].

If the GaN buffer is very thin, the surface of c-GaN films will be rough and the thermal decomposition. During the growth process of c-GaN films, high operating will occur destroys surface of GaAs substrate which lead to void area at the interface between c-GaN films and GaAs substrate. Sormunen et al. [24] reported the thickness 8 nm of LT-GaN buffer layer at 600 °C that could produce smooth surface c-GaN films on GaAs (100).

### 2.3 Selective Area Growth (SAG)

Selective area growth is also a method to reduce dislocation density within windows or open width area. Because stacking faults (SFs) and threading dislocation lines (TDs) occur at the interface of film and substrate. There are two types which are dot and line patterns, as shown in Fig. 2.6.

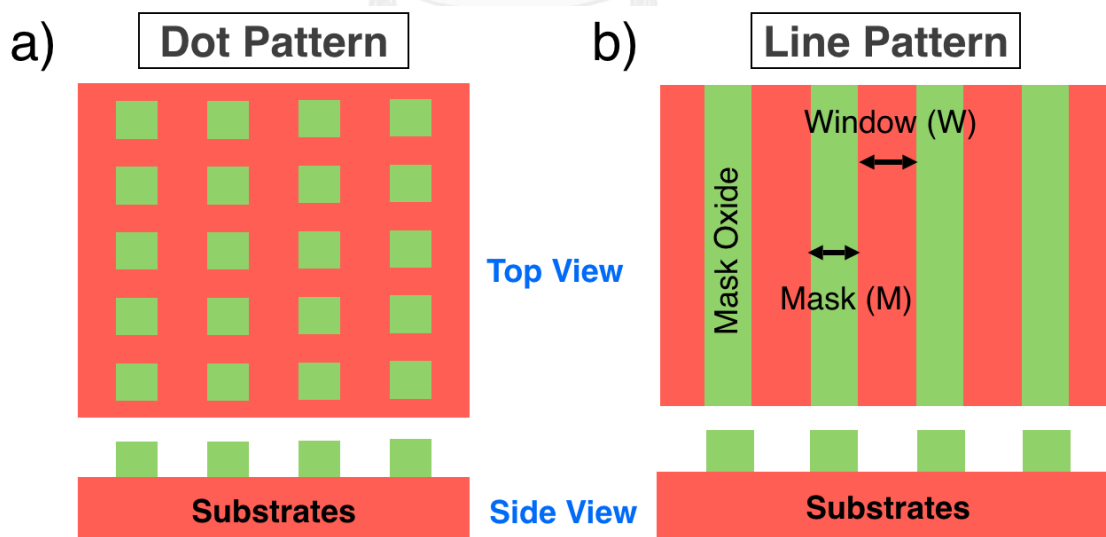


Figure 2.6: Top and side view of SAG c-GaN with a) dot and b) line patterns (green color - mask and orange color - windows or open width area).

### 2.3.1 Dot Pattern

Shen et al. [25] reported c-GaN grown on GaAs (001) with dot pattern template that the density of SFs was reduced to  $6 \times 10^8 \text{ cm}^{-2}$  compared with dot pattern template with SF density of  $5 \times 10^9 \text{ cm}^{-2}$ . The SFs were blocked under  $\text{SiO}_2$  mask layer, as shown in Fig. 2.7.

Because of c-GaN on dot pattern were generated along [1-10] and [110] windows stripe, the c-GaN growth films have two different dominant facets generating which were (111)B and (111)A that had different morphologies of c-GaN films [26]. The SAG with line pattern is another method to reduce SF density in the c-GaN generating from the two directions of dot pattern. By using SAG with line pattern, it was reducing mix GaN generating between (111)B and (111)A which reduced SFs in the c-GaN films.

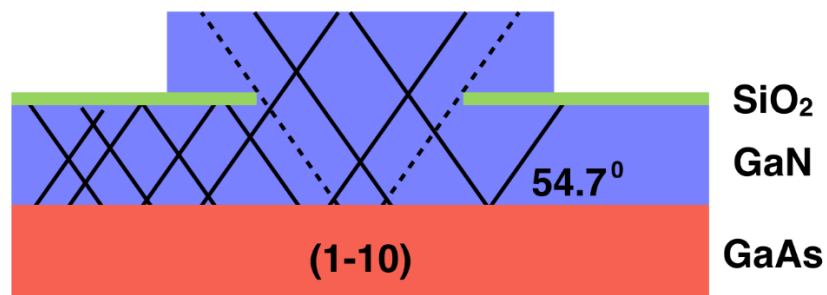


Figure 2.7: Schematic diagram of reduction mechanism of SFs during ELO of cubic GaN [25].

### 2.3.2 Line Pattern

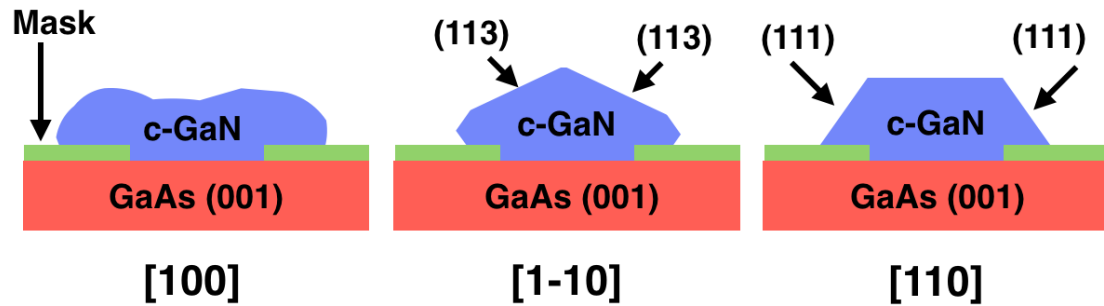


Figure 2.8: Morphologies of SAG c-GaN films along to the [100], [1-10] and [110] mask stripe directions.

The facet lateral epitaxial lateral overgrowth (FACELO) depends on mask stripe directions. In Fig. 2.8, the growth morphologies of c-GaN along to the [100], [1-10] and [110] mask directions on GaAs (001) substrates [27-29]. The morphology of c-GaN on [100] mask pattern GaAs (001) showed unclear sidewall facet. The dominant (113) sidewall facets of c-GaN showed on [1-10] mask pattern GaAs (001) that was dominant cubic phase purity for this c-GaN plane facets. The dominant (111) sidewall facets of c-GaN showed on [110] mask pattern GaAs (001) which are related to (111) c-GaN // (10-11) h-GaN.

### 2.4 Epitaxial Lateral Overgrowth (ELO)

Epitaxial lateral overgrowth (ELO) is the method that followed SAG method. Normally, the film grows with higher vertical growth rate than lateral growth rate at the beginning of growth process. The growth models of ELO c-GaN on [1-10] and [110] mask pattern GaAs (001) were shown on Fig 2.9.

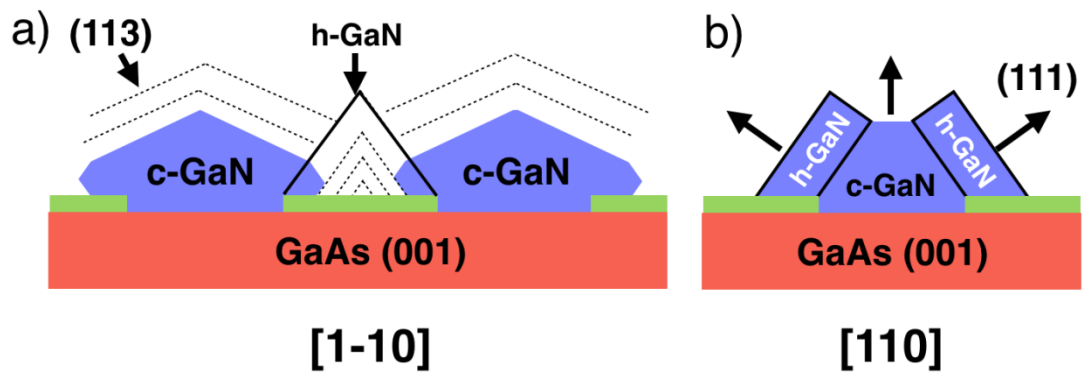


Figure 2.9: Growth models of ELO c-GaN on (a) [1-10] and (b) [110] mask pattern GaAs (001) [28, 29].

The lateral growth mechanism on mask area showed h-GaN structure for both mask patterns on GaAs (001). On [1-10] mask pattern, ELO c-GaN had (113) dominant sidewall facets and (111) sidewall at the edge of c-GaN stripe. When the c-GaN stripes merged together, (111) sidewall facets which h-GaN as dominant structure were limited under (113) dominant sidewall facets which c-GaN as dominant structure. While on [110] mask pattern, (111) h-GaN sidewall facets were increasing for longer growth time and covered c-GaN structure on open width area.

## 2.5 Mask Fill Factor

Mask fill factor (FF) is the length ratio of windows (W) or open width area to the period or mask area (M) and windows (W), as shown in Fig. 2.10.

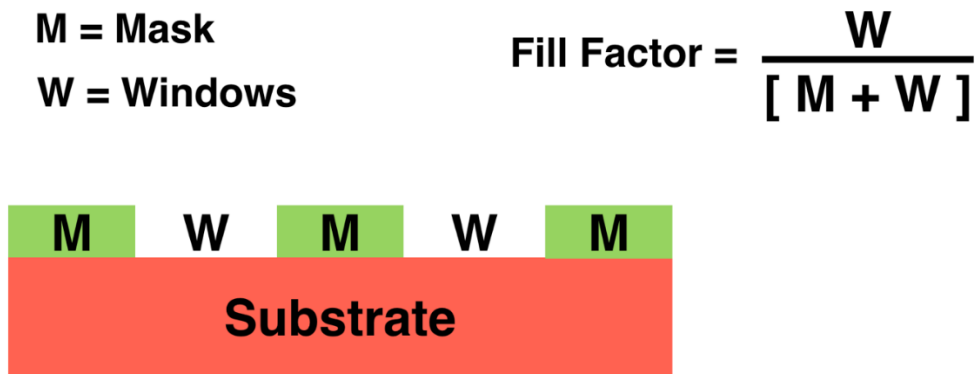


Figure 2.10: Mask fill factor [M – mask area and W - windows or open width area].

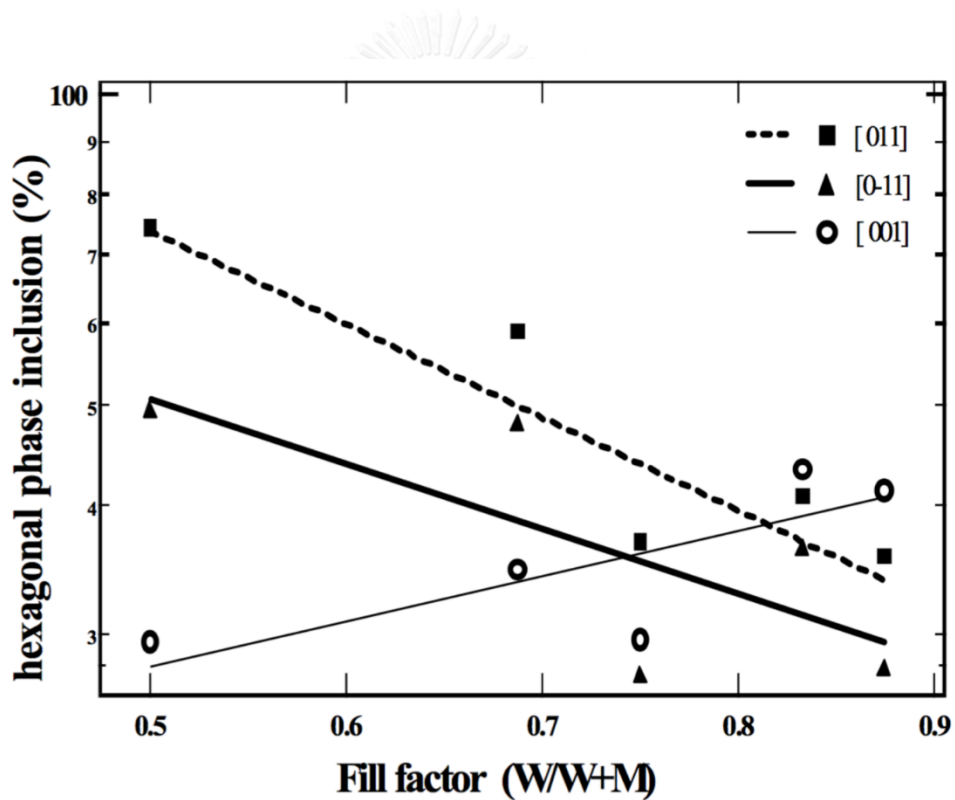


Figure 2.11: Dependence of the hexagonal phase inclusion on the fill factor [30].

Mask fill factor is an important parameter to control cubic phase GaN. There is not much reported about FF. The relationship of hexagonal phase inclusion and FF for c-GaN on [001], [0-11] and [011] mask pattern GaAs (001) were reported by

Sanorpim et al. [30]. The results showed that the hexagonal phase inclusion was increasing during FF 0.5 to 0.9 for [001] mask pattern GaAs (001). While [0-11] and [011] mask pattern GaAs (001), The hexagonal phase inclusion was decreasing during FF from 0.5 to 0.9, as shown in Figure 2.11. The FF between 0.7 and 0.8 had the lowest hexagonal phase inclusion for [1-10] and [110] mask pattern on GaAs (001).

## 2.6 Growth Temperature

The growth temperature of c-GaN films is also the key parameters to control cubic phase GaN films. The crystal quality and hexagonal phase inclusion of each mask stripe directions depends on the growth temperature. Sanorpim et al. [27] reported the effect of growth temperature for SAG c-GaN on [011] and [001] mask stripe pattern GaAs (001). The growth morphologies of SAG c-GaN on [011] mask stripe pattern were changed to (811)B side wall facets at the top when growth temperature was increased more than 900 °C, as shown in Fig 2.12. While the SAG c-GaN on [001] mask stripe pattern had no different growth morphologies with increasing growth temperature from 900 to 960 °C, the growth morphologies had unclear sidewall facets due to rough surface on the top and side. The FWHM in rocking curve mode and hexagonal phase inclusion were increased when the growth temperature was increasing. With SAG c-GaN on [001] mask stripe pattern on GaAs (001), the results of FWHM in rocking curve mode and hexagonal phase inclusion were decreased when the growth temperature was increased. The optimised suitable growth temperature was 900 °C which SAG c-GaN on [011] mask stripe pattern GaAs (001) achieved the highest cubic phase purity GaN more than 85%. The growth temperature effect was also studied by ED patterns in TEM which showed SFs in c-

GaN on GaAs (001) [31]. The h-GaN structure was clearly observed at the growth temperature more than 930 °C while no diffraction from ED pattern was observed for h-GaN at growth temperature of 900 °C.

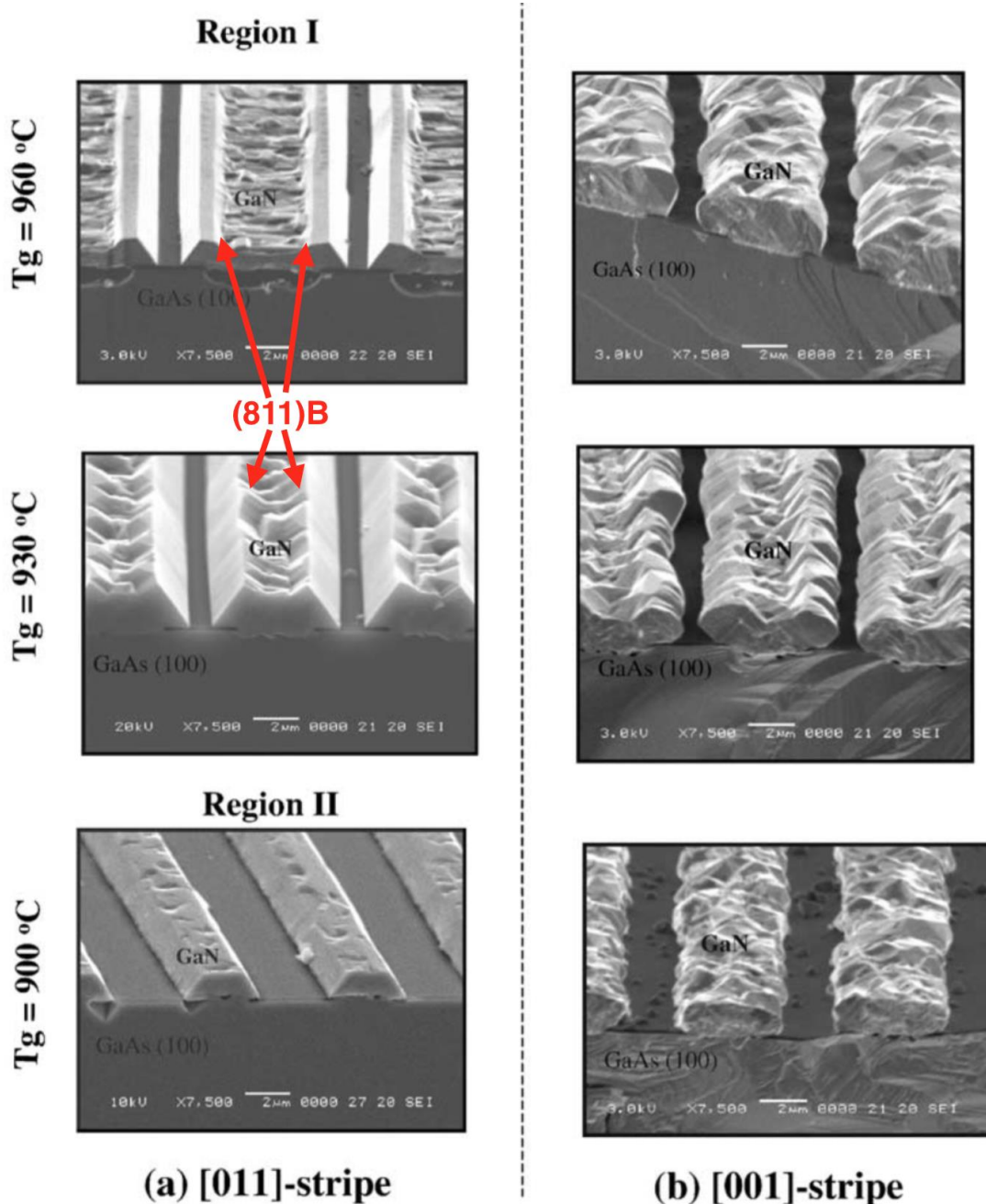


Figure 2.12: Growth features of SAG c-GaN on (a) [011] and (b) [001]-stripe pattern for different growth temperature [27].

## CHAPTER III

### GROWTH PROCESS AND CHARACTERIZATION

#### 3.1 MOVPE Growth Process

SAG/ELO cubic GaN were grown by MOVPE on [100], [1-10] and [110] mask patterned GaAs (001) by MOVPE. The growth times were 10, 30, 60 and 120 minutes. The descriptions of growth process and characterization methods were shown as follows.

##### 3.1.1 Mask Stripe Directions

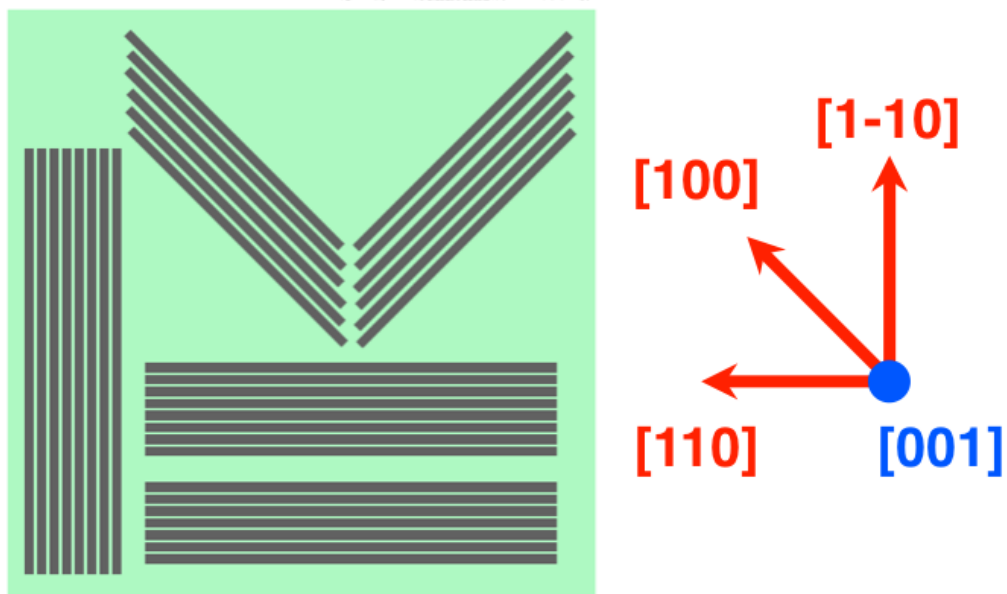


Figure 3.1: Mask pattern along [100], [1-10] and [110] directions on GaAs (001) substrate (green color - mask oxide and grey color - windows area).

The mask stripe pattern on GaAs (001) along [100], [1-10] and [110] directions showed in Fig. 3.1. The red arrows indicate the directions of mask patterns and the blue point is [001] azimuth axes. The process was started from the 200 nm thick silicon dioxide which were deposited by RF sputtering. The [100], [1-10] and [110] mask stripe patterns were created by UV photolithography following with wet chemical etching. Growth evolution time of the ELO c-GaN films was studied for each mask stripe directions.

### 3.1.2 ELO c-GaN Film Growth Process

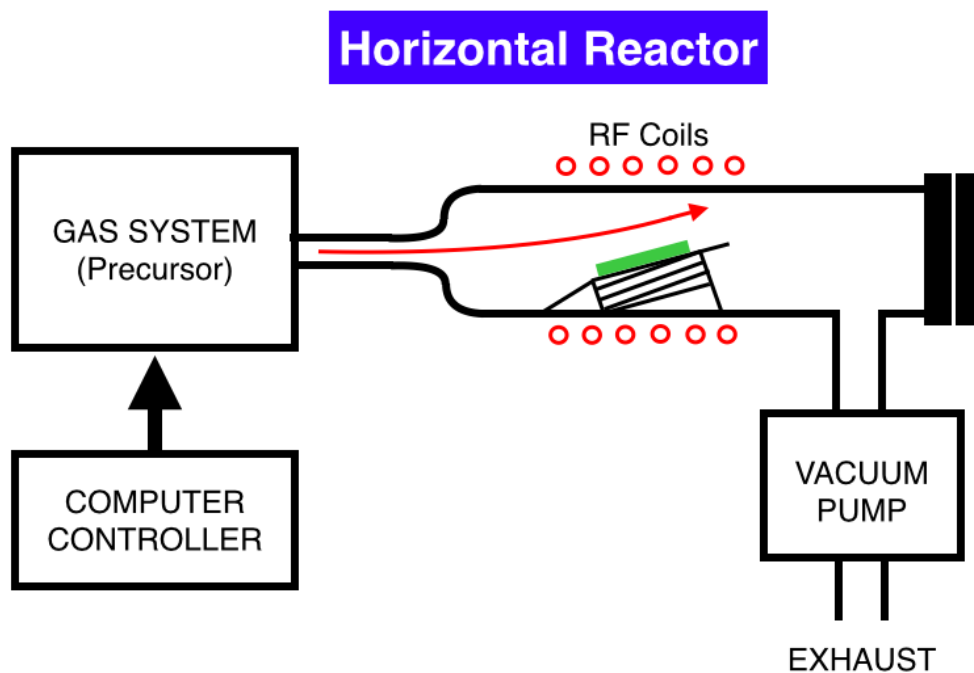


Figure 3.2: The horizontal reactor of MOVPE system.

The GaAs (001) substrate with oxide mask layer was loaded inside the horizontal reactor type of MOVPE system, as shown in Fig. 3.2. This MOVPE system was controlled by computer controller to adjust the precursor gases by controlling flow rate and pressure in the reactor. hydrogen ( $H_2$ ) was used as carrier gas was to flow precursor gas to horizontal reactor. Trimethylgallium (TMGa), 1-1-dimethylhydrazine (DMhy) and tertiarybutylarsine (TBAs) were used as precursor gas sources for Ga, N and As, respectively. The vacuum pump was used to maintain gas pressure at 160 Torr. The radiofrequency (RF) coils were the heater to heat the reactor and the temperature were control by thermocouple which located under substrate.

The growth process with double buffer layers and c-GaN films were shown in Fig. 3.3. After the masked GaAs (001) substrate with mask patterns was loaded in horizontal reactor, double buffer layers consisted of GaAs and c-GaN were grown to reduce lattice mismatch, thermal decomposition and control cubic phase GaN at the interface between c-GaN films and GaAs (001) substrates.

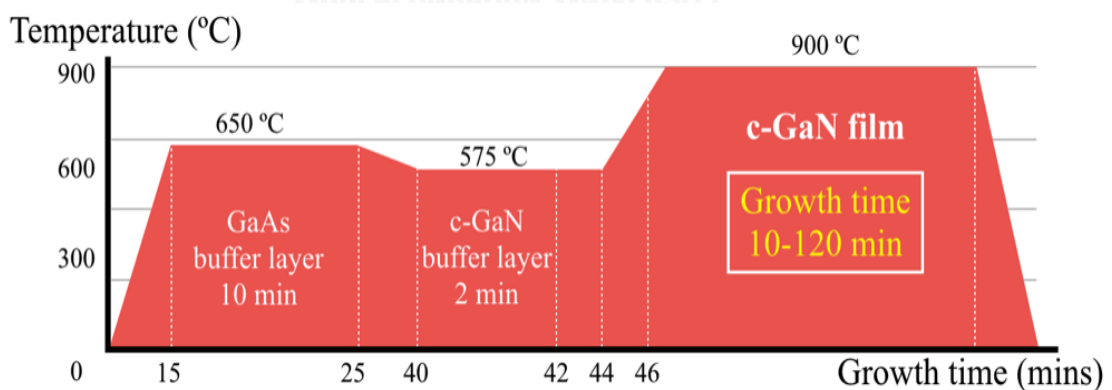


Figure 3.3: Growth temperature and growth time process of ELO c-GaN with double buffer layers.

The growth temperature in reactor was increased from room temperature to 650 °C during 15 minutes to prepare the growth of GaAs buffer layer. GaAs buffer layer was grown at 650 °C with V/III (As/Ga) ratio of 15 for 10 minutes which the thickness of GaAs buffer layer was 100 nm. After that the temperature was decreased to 575 °C within 15 minutes to prepare the growth of c-GaN buffer layer. The c-GaN buffer layer was grown at low temperature of 575 °C with V/III (N/Ga) ratio of 100 for 2 minutes of which the thickness of LT-GaN buffer layer was 20 nm.

The reason for using low temperature as 575 °C to grow c-GaN buffer layer is because the thermal decomposition would damage the GaAs buffer layer and GaAs substrates. Then the growth temperature was kept steady at 575 °C for 2 minutes before the growth temperature was increasing to 900 °C with ramping time for 2 minutes before the growth process of c-GaN films. The growth parameters of c-GaN films were V/III ratio of 25, growth operating temperature at 900 °C, the growth time of 10, 30, 60 and 120 minutes and the pressure steady at 160 Torr. The growth temperature of 900 °C was optimized to produce high cubic phase purity with smooth surface of the c-GaN films [14].

### 3.1.3 Sample Structure

The total samples were four pieces for the growth time of 10, 30, 60 and 120 minutes. The sample structure on GaAs (001) consisted of 200-nm thickness mask and double buffer layer of 100-nm thickness GaAs and 20-nm thickness LT-GaN with c-GaN films at the growth time of 10 to 120 minutes on window area, as shown in Fig. 3.4.

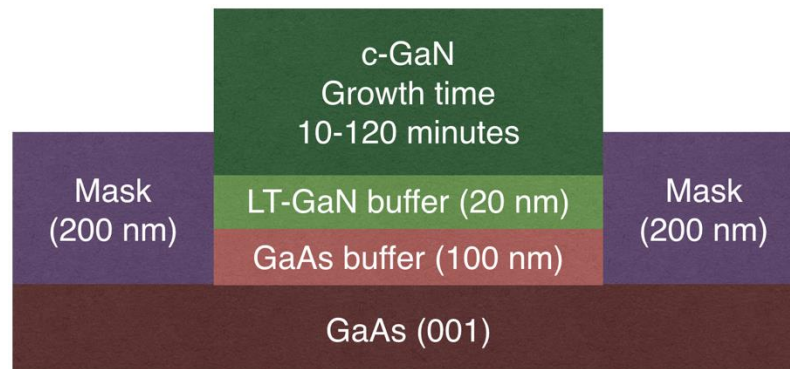


Figure 3.4: Sample structure of c-GaN on GaAs (001) with mask stripe pattern and double buffer layers of LT-GaN and GaAs.

The thickness of c-GaN films at the growth time of 10 to 120 minutes were characterized by SEM. Each sample had three mask stripe directions which were [100], [1-10] and [110]. So, the total of samples for characterizations were twelve pieces. All of samples were grown at Onabe's Laboratory, department of Advanced Material Science, The University of Tokyo.

### 3.2 Characterization Techniques

All of samples were analyzed by SEM to study growth morphologies which depends on growth time evolution for each mask stripe directions. Then micro-Raman spectroscopy was used to indicate the specific spot area on c-GaN films to confirm the cubic and hexagonal GaN structures. HRXRD was used to verify cubic and hexagonal GaN structure, quality of the c-GaN films and hexagonal phase inclusion.

### 3.2.1 Scanning Electron Microscope (SEM)

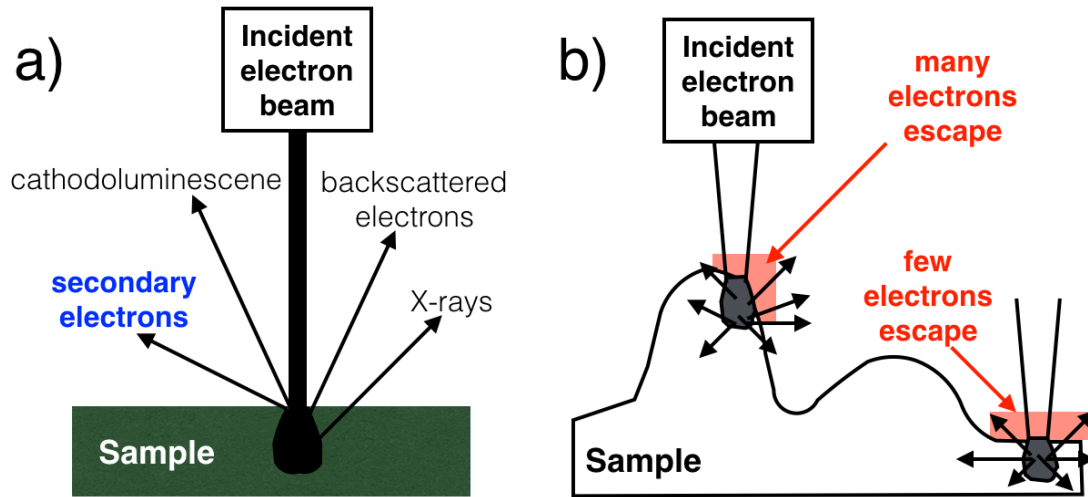


Figure 3.5: (a) Signal of incident electron beam to sample and (b) secondary electrons on different surface on sample.

The incident electron beam to the sample caused many signals, as shown in Fig. 3.5 (a). SEM images come from secondary electrons which depends on secondary electrons escape from the surface of sample. In Fig. 3.5 (b), the details of secondary electrons for different morphologies surface show that many electrons can escape from curve surface more than flat surface which only few electrons can escape. The contrast of secondary electrons at edges is called edge effect that can investigate surface morphology and surface topology of the films.

The SEM images were taken from JEOL JSM-7001F operated at acceleration voltage of 20 kV from The Scientific and Technology Research Equipment Center (STREC), Chulalongkorn University. The overview of surface topology was analyzed from plane view SEM images with magnifications of 2000 and 6000 times at the growth time of 10, 30, 60 and 12 minutes for [100], [1-10] and [110] mask stripe

directions. Their growth morphologies especially sidewall facets of c-GaN films were investigated by cross-sectional SEM images with magnifications of 2000 and 6000 times. The thickness of the c-GaN films and the growth rate also find from cross-sectional SEM images.

### 3.2.2 Micro-Raman Scattering

There are two possible ways of light scattering which are elastic and inelastic scattering. Rayleigh scattering or elastic scattering occurs the scattering photons have the same energy as incident photon (frequency and wavelength) while inelastic scattering are Stokes and anti-Stokes scattering, as shown in Fig. 3.6.

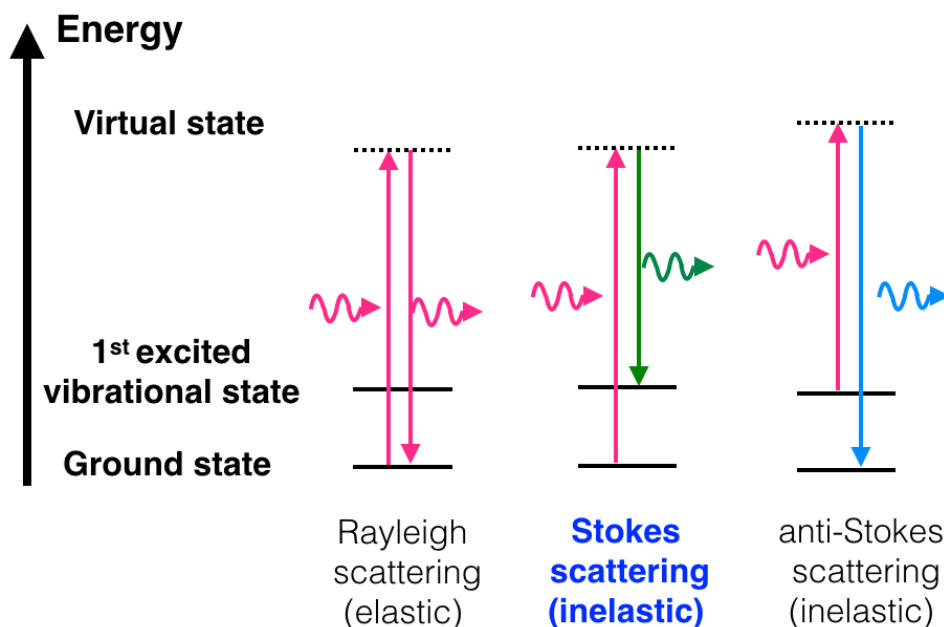


Figure 3.6: Energy diagram of Rayleigh scattering, Stokes and anti-Stokes Raman scattering.

Table 3.1: Phonon modes in cubic and hexagonal GaN

<b>c-GaN/ on</b>	<b>GaAs [32]</b>	<b>3c-SiC/Si [33]</b>	<b>GaAs [34]</b>	<b>GaAs [35]</b>	<b>GaAs [36]</b>
TO ( $\text{cm}^{-1}$ )	553	551	555	553	554
LO ( $\text{cm}^{-1}$ )	739	735	741	740	739
<b>h-GaN/ on</b>	<b>GaAs [32]</b>	<b>3c-SiC/Si [33]</b>	<b>GaAs [34]</b>	<b>Sapphire [37]</b>	<b>Sapphire [38]</b>
A <sub>1</sub> (TO) ( $\text{cm}^{-1}$ )	-	538	537	-	532
E <sub>1</sub> (TO) ( $\text{cm}^{-1}$ )	-	-	556	-	559
E <sub>2</sub> high ( $\text{cm}^{-1}$ )	568	565	571	570	568
A <sub>1</sub> (LO) ( $\text{cm}^{-1}$ )	733	-	737	735	734
E <sub>1</sub> (LO) ( $\text{cm}^{-1}$ )	-	-	-	-	741

The energy of incident photon is decreased because of energy transfer to vibrate in the atoms or crystal structures which called Raman shift ( $\text{cm}^{-1}$ ). Normally, Anti-Stokes is rarely measured due to less intensity than the Stokes. However, it is equivalent with Stokes for the vibration in crystal structures. The Raman shift is the unique value to detect crystal structures.

The cubic phase and hexagonal phase for Stokes scattering is shown in Table 3.1 which unique vibrational mode for each structures of c-GaN on GaAs and 3c-SiC/Si and h-GaN on GaAs, sapphire and 3c-SiC/Si. Cubic phase GaN have phonon vibrational modes of longitudinal optical (LO) and transverse optical (TO) while hexagonal phase GaN have  $A_1$  (TO),  $E_1$  (TO),  $E_2$  high,  $A_1$  (LO) and  $E_1$  (LO) phonon vibrational modes.

Reinshaw Ramanscope RM1000 was an instrument to measure Raman Spectra operating by the Gem and Jewellery Institute of Thailand (Public Organization), Chulalongkorn University. The monochromatic high frequency light source of 514.5-nm line of Ar<sup>+</sup> ion laser was operating at room temperature. The micro-Raman scattering spectroscopy was used to detect cubic or hexagonal GaN phonon vibrational modes on specific area that spot size  $\sim 2 \mu\text{m}$ . The Raman spectra were measured in backscattering geometry. The range of wavenumber was 250-800  $\text{cm}^{-1}$  which covered GaAs TO and LO modes.

Since c-GaN films were grown on [100], [1-10] and [110] mask stripe pattern on GaAs (001), the growth morphologies for each mask stripe pattern had different shape and sidewall facets. The relationship of growth time evolution was investigated by the top and sidewall facets for various mask stripe directions.

### 3.2.3 High Resolution X-ray Diffraction (HRXRD)

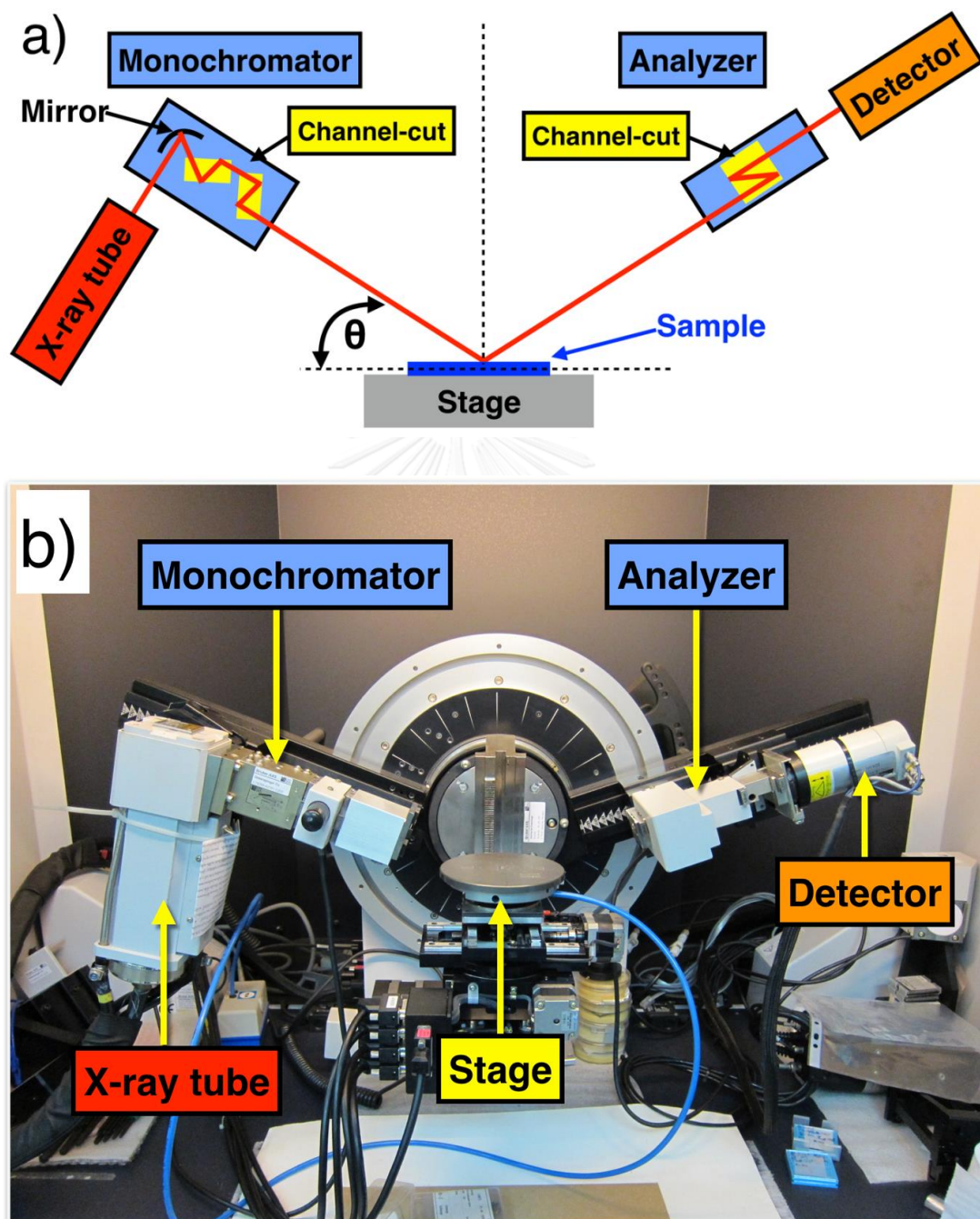


Figure 3.7: (a) Illustrated of HRXRD and (b) photo of Bruker-AXS Discover D8 in High resolution mode.

HRXRD is an instrument to measure the epitaxial layer. The data information gives details of crystal structure, lattice constant, crystal orientation, mosaic and phase inclusion. HRXRD data were collected from Bruker-AXS D8 Discover with  $\text{CuK}\alpha_1$  beam source wavelength  $1.5406 \text{ \AA}$ , at operating acceleration voltage  $40 \text{ kV}$  which is located at the Scientific and Technology Research Equipment Center (STREC), Chulalongkorn University. Bruker-AXS D8 Discover has four-crystal Ge (022) as channel-cut monochromator which  $\Delta\omega \sim 0.003^\circ$  in front of X-ray source and two-crystal Ge (022) as channel-cut analyzer which  $\Delta 2\theta \sim 0.003^\circ$  in front of detector, as shown in Fig 3.7. The monochromized beam is  $\Delta\lambda/\lambda = 0.0003$  ( $\Delta\lambda$  - the spectral width of the X-ray beam) which any crystal can be measured. The basic of X-ray with Bragg's law is shown in Fig. 3.8.

$$\lambda = 2d_{hkl} \sin \theta_B \quad (3.1)$$

where  $d_{hkl}$  is the lattice plane spacing (d-spacing) of the hkl plane,  $\theta_B$  is the Bragg's angle and  $\lambda$  is the wavelength of X-ray which is  $1.5406 \text{ \AA}$  for  $\text{CuK}\alpha_1$  beam source.

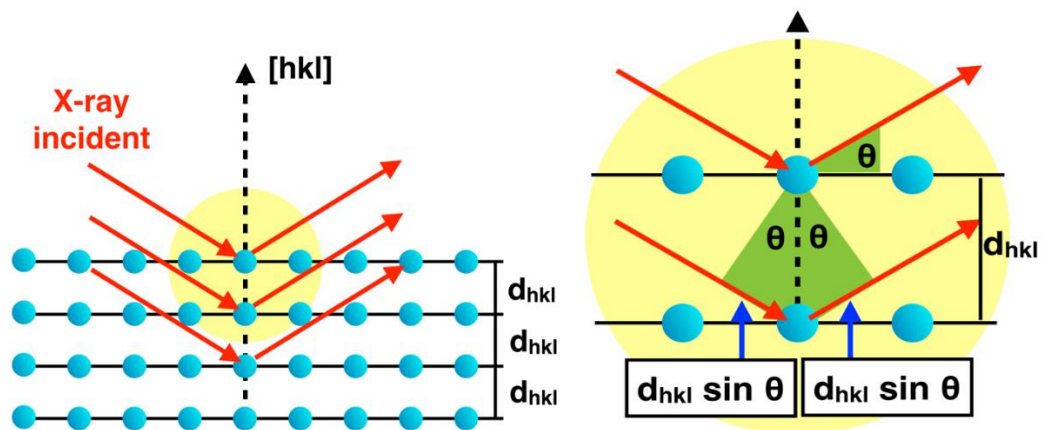


Figure 3.8: X-ray with Bragg's law.

The data of HRXRD for investigation were obtained from  $2\theta/\omega$ -scan, rocking curve ( $\omega$ -scan) and reciprocal space mapping modes.

### 3.2.3.1 $2\theta/\omega$ -scan mode

In  $2\theta/\omega$ -scan mode, lattice plane spacing is measured. The range of  $2\theta/\omega$  is 31 to 41 degrees. The dominant peak of GaAs (002) and c-GaN (002) with small peaks or no peak of h-GaN (10-11) and h-GaN (0002) were observed. The normalized GaAs (002) peak for each mask stripe directions was investigated at the growth time of 10, 30, 60 and 120 minutes. The FWHMs of  $\Delta(2\theta/\omega)$ , which shows the result of strain in the c-GaN films, were compared among different growth time and mask stripe directions.

### 3.2.3.2 Rocking curve ( $\omega$ -scan) mode

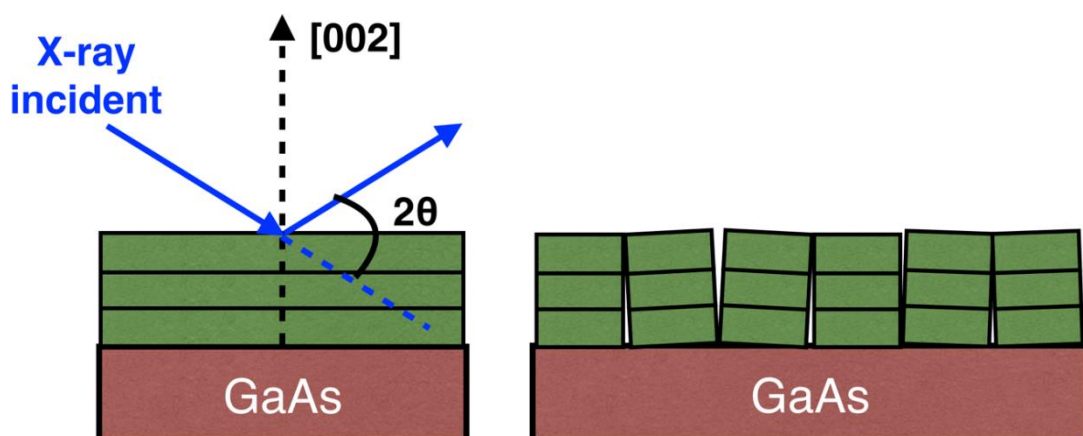


Figure 3.9: Rocking curve mode ( $\omega$ -scan) of c-GaN (002).

The rocking curve mode ( $\omega$ -scan) shows the mosaic of c-GaN, as shown in Fig. 3.9. The broader peak of FWHM is referred to a lot of mosaics. The  $\omega$ -scan of c-GaN (002) were measured in the two directions which are X-ray incident beam perpendicular and parallel with mask stripe directions. The results of FWHM were compared by growth time, mask stripe directions and directions of X-ray beam with mask stripe patterns.

### 3.2.3.3 Reciprocal space mapping (RSM) mode

The reciprocal space mapping mode is the HRXRD scanning in  $2\theta/\omega$  and  $\omega$ . The defects in c-GaN films can be analysed from the board of c-GaN (002), show in Fig. 3.10 (a). Strain is broadening along ( $2\theta/\omega$ )-scan while tensile strain is broadening along  $\omega$ -scan. There are two possible types of tensile strain which are mosaic and misfit. Mosaic is board area in curve along to  $\omega$ -scan and misfit is board area at the straight direction of  $\omega$ -scan. For symmetrical RSM of c-GaN (002), h-GaN {10-11} found at  $\omega \sim 7^\circ$ , as shown in Fig. 3.10 (b).

The hexagonal phase inclusion was calculated from integrated intensities of c-GaN (002) and h-GaN {10-11} with X-ray incident beam perpendicular and parallel with mask stripe patterns.

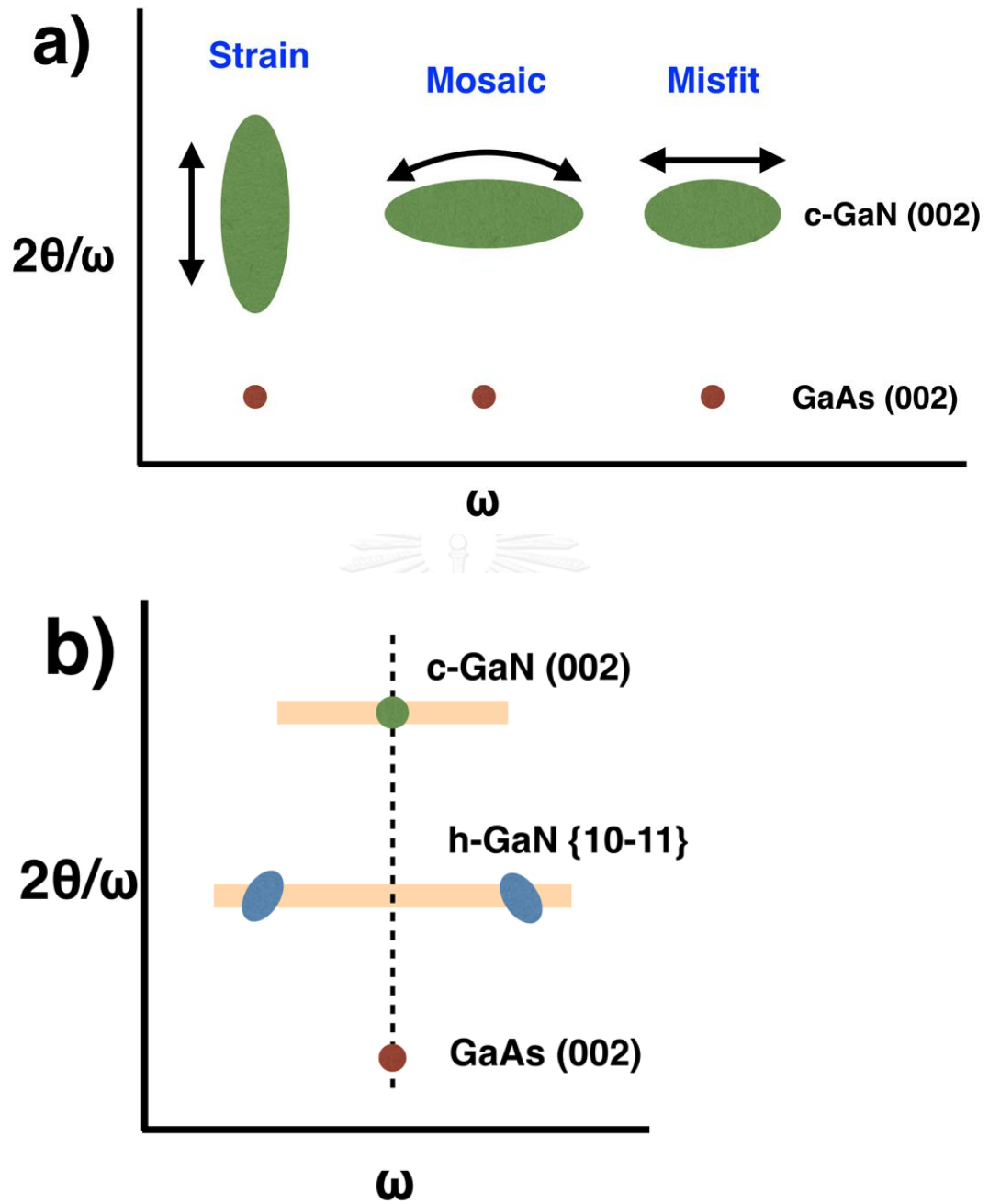


Figure 3.10: Symmetrical RSM mode of c-GaN (002) on GaAs (a) type of defects and (b) hexagonal phase inclusion {10-11}.

Table 3.2: Theoretical calculation X-ray intensities of c-GaN (002) and h-GaN (10-11) [39, 40].

Structures	Planes	Degrees	I (10 <sup>5</sup> cps)	I/I <sub>c</sub> (002)
Cubic	(002)	19.9	8.41	1.00
Hexagonal	(10-11)	18.4	8.97	<b>1.07</b>

The theoretical integrated XRD intensities  $I$  are given by

$$I = I_0 \times |F(hkl)|^2 \times P \times V \times L_p \times N^2 \times e^{-2M} \quad (3.2)$$

where  $I_0$ ,  $F(hkl)$ ,  $P$ ,  $V$ ,  $L$ ,  $N$  and  $e^{-2M}$  are incident intensity, structure factor, multiplicity factor, volume, Lorentz polarization factor, a number of unit cell per unit volume and temperature, respectively. The results of theoretical calculation X-ray intensities are show in Table 3.2.

The weight factor ( $\alpha$ ) of  $I_{h-(10-11)}/I_{c-(002)}$  was calculated from theoretical calculation X-ray intensities of c-GaN (002) and h-GaN (10-11) which are 1.07.

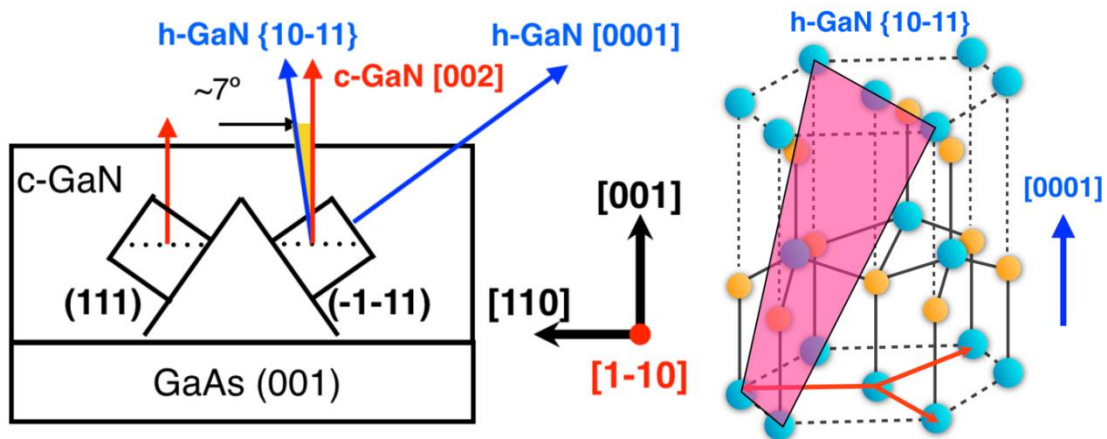


Figure 3.11: c-GaN on GaAs (001) with family plane of {111} [1-10] azimuth axes.

The reason of measuring X-ray incident beam perpendicular and parallel directions with mask stripe patterns because of family plane of {111} like pyramid shape. The [1-10] and [110] azimuth axes of c-GaN on GaAs (001) have the hexagonal phase inclusion can generate at (111), (-1-11), (1-11) and (-111) plane. As shown in Fig. 3.11, (111) and (-1-11) c-GaN on GaAs (001) with cross-sectional view of [1-10] azimuth axis show h-GaN structure on (-1-11) c-GaN plane.

The hexagonal phase inclusion is calculated from the integrated X-ray intensities of h-GaN (10-11) and c-GaN (002) as follow.

$$V_h = \frac{I_h}{I_{0-h} \times |F(hkl)|_h^2 \times P_h \times L_{P-h} \times N_h^2 \times e_h^{-2M}} \quad (3.3)$$

$$\frac{V_h}{V_c} = \frac{I_h \times I_{0-c} \times |F(hkl)|_c^2 \times P_c \times L_{P-c} \times N_c^2 \times e_c^{-2M}}{I_c \times I_{0-h} \times |F(hkl)|_h^2 \times P_h \times L_{P-h} \times N_h^2 \times e_h^{-2M}} \quad (3.4)$$

$$\%V_h = \frac{V_h/V_c}{1+V_h/V_c} \times 100\% \quad (3.5)$$

$$\%V_{h-GaN} = \frac{I_{h-GaN(10-11)}}{I_{h-GaN(10-11)} + \alpha \bar{I}_{c-GaN(002)}} \times 100 \quad (3.6)$$



## CHAPTER IV

### EXPERIMENTAL RESULTS

The experimental results are described with the instruments that collected the data. The images from optical microscope (OM) show overview of samples with [100], [1-10] and [110] mask stripe directions. The SEM images were collected for plane view and cross-sectional view to observe the growth morphology and topology of SAG/ELO c-GaN films. Raman spectra from micro-Raman scattering microscopy show the Raman intensities related to cubic and hexagonal GaN structures. The results of HRXRD come from  $(2\theta/\omega)$ -scan,  $\Delta(2\theta/\omega)$ ,  $\omega$ -scan and reciprocal space mapping modes.

#### 4.1 Optical Image

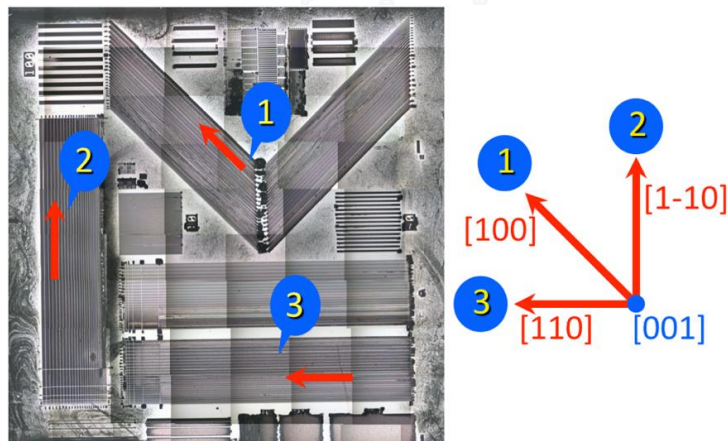


Figure 4.1: Multiple optical microscopy images of SAG/ELO c-GaN on GaAs (001) at growth time of 10 min (sample size 11.4 x 9.9 mm).

As shown in Fig. 4.1, the combination of multiple OM images shows the overview of sample which red arrows indicate the mask stripe directions of [100], [1-10] and [110] on GaAs (001) with the number of 1, 2 and 3, respectively. The azimuth axis is [001] direction which indicate in blue color.

The overall OM images with 500 times magnification for SAG/ELO c-GaN films along [100], [1-10] and [110] mask stripe directions GaAs (001), as shown in Fig. 4.2. On the [100] direction, shown in Fig. 4.2 (a-d), the SAG/ELO c-GaN films on window area have merged together on the mask area at the growth time more than 60 minutes. The top surface appeared rough SAG/ELO c-GaN film.

In the case of [1-10] and [110] directions, as shown in Fig. 4.2 (e-l), the individual of SAG/ELO c-GaN stripe films have observed at the growth time of 10 to 120 minutes which mean the SAG/ELO do not have the smooth flat facets on the top at the growth time of 120 minutes. The shape of SAG/ELO c-GaN films are different morphologies which see from the contrast colors. On the [1-10], the SAG/ELO c-GaN stripe films on windows area are clearly observed the rough sidewall facets at the growth time of 60 minutes. Then the smoother sidewall facets of SAG/ELO c-GaN films are observed at the growth time of 120 minutes. The shape of SAG/ELO c-GaN film seem to be the triangle shape because the top surface cannot observe.

On the [110] direction, the SAG/ELO c-GaN films on windows area appear the smooth flat surface at the growth time of 10 minutes and more rough surface with some cracks at growth time of 60 minutes. The top surface becomes smoother with lower cracks with the direction of the cracks perpendicular with mask stripe direction at the growth time of 120 minutes.

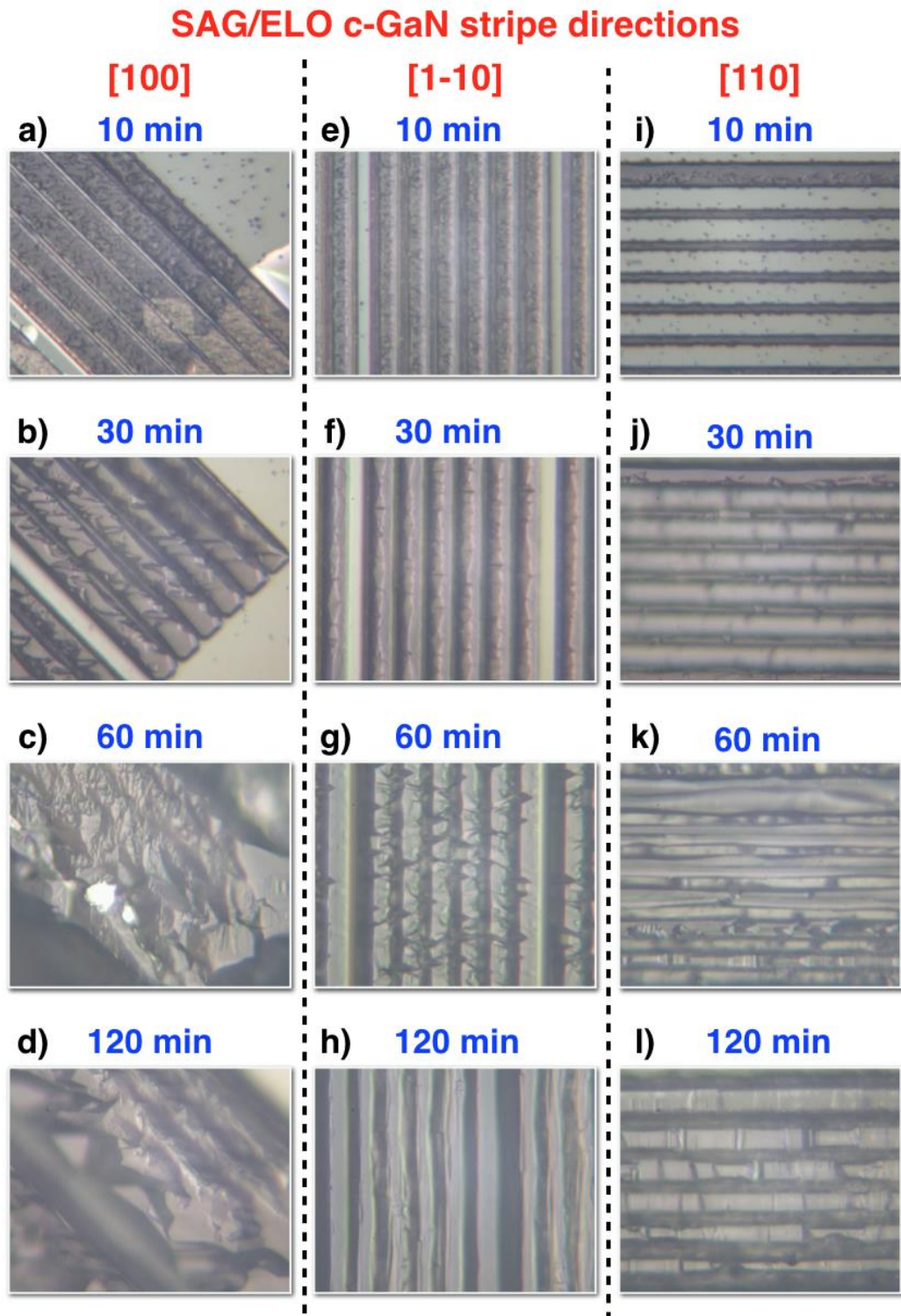


Figure 4.2: Optical microscope images (500x) of SAG/ELO c-GaN films on (a-d) [100], (e-h) [1-10] and (i-l) [110] mask pattern GaAs (001) at growth time of 10, 30, 60 and 120 min.

## 4.2 Scanning Electron Microscopy (SEM)

Scanning electron microscopy (SEM) images were collected from plane view and cross-sectional view. The plane view of SEM images shows the surface of SAG/ELO c-GaN films while cross-sectional view SEM images shows the detail of growth morphologies of SAG/ELO c-GaN films for each mask stripe directions.

The plane view SEM images with 2000 times of magnification are shown in Fig. 4.3. On the [100] direction, the c-GaN films on window area are merged together at the growth time of 60 minutes with very rough surface and large crack sizes observed at the growth time of 120 minutes, i.e. similar results from OM images. On the [1-10] direction, shown in Fig. 4.3 (e-h), the rougher top surface is shown as growth time is increased from 10 to 60 minutes. However, the sidewall facets show smooth surface with little crack at the peak of c-GaN films at the growth time of 120 minutes that mean the SAG/ELO c-GaN films become more uniform than at the growth time of 60 minutes. The smooth top surfaces are shown on [110] mask stripe direction with smooth sidewall facets, as shown in Fig. 4.3 (i-l). On the top of SAG/ELO c-GaN films, the crack lines are observed at the growth time of 60 to 120 minutes.

Cross-sectional view of SEM images with 2000 times of magnification of SAG/ELO c-GaN on GaAs (001) are shown in Fig. 4.4. The samples were cut to measure the thickness and the shape of SAG/ELO c-GaN films. The growth morphologies of SAG/ELO c-GaN on [100] mask stripe patterned show the top rough facet at (001) plane, as shown in Fig 4.4 (a-d). The SAG/ELO c-GaN films on windows area were merged together during the growth time of 30 to 60 minutes. The average thickness of SAG/ELO c-GaN film is increasing from  $\sim 1.8 \mu\text{m}$  at the growth time of 10 minutes to  $\sim 11 \mu\text{m}$  at the growth time of 120 minutes.

## 4.2.1 Plane View of SEM Images

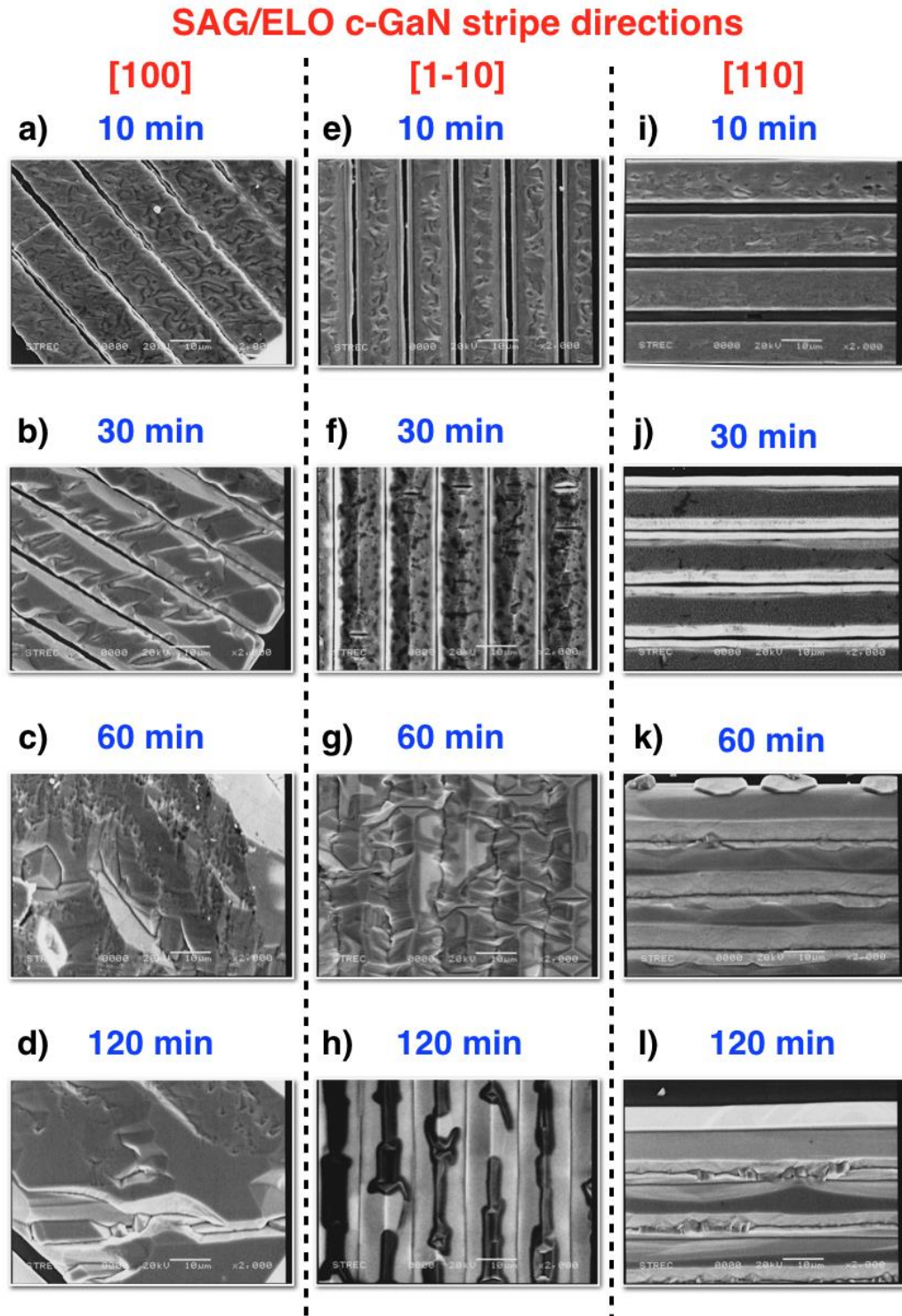


Figure 4.3: Plane view SEM images of SAG/ELO c-GaN on (a-d) [100], (e-h) [1-10] and (i-l) [110] mask pattern GaAs (001) at the growth time of 10 to 120 min.

## 4.2.2 Cross-sectional View of SEM Images

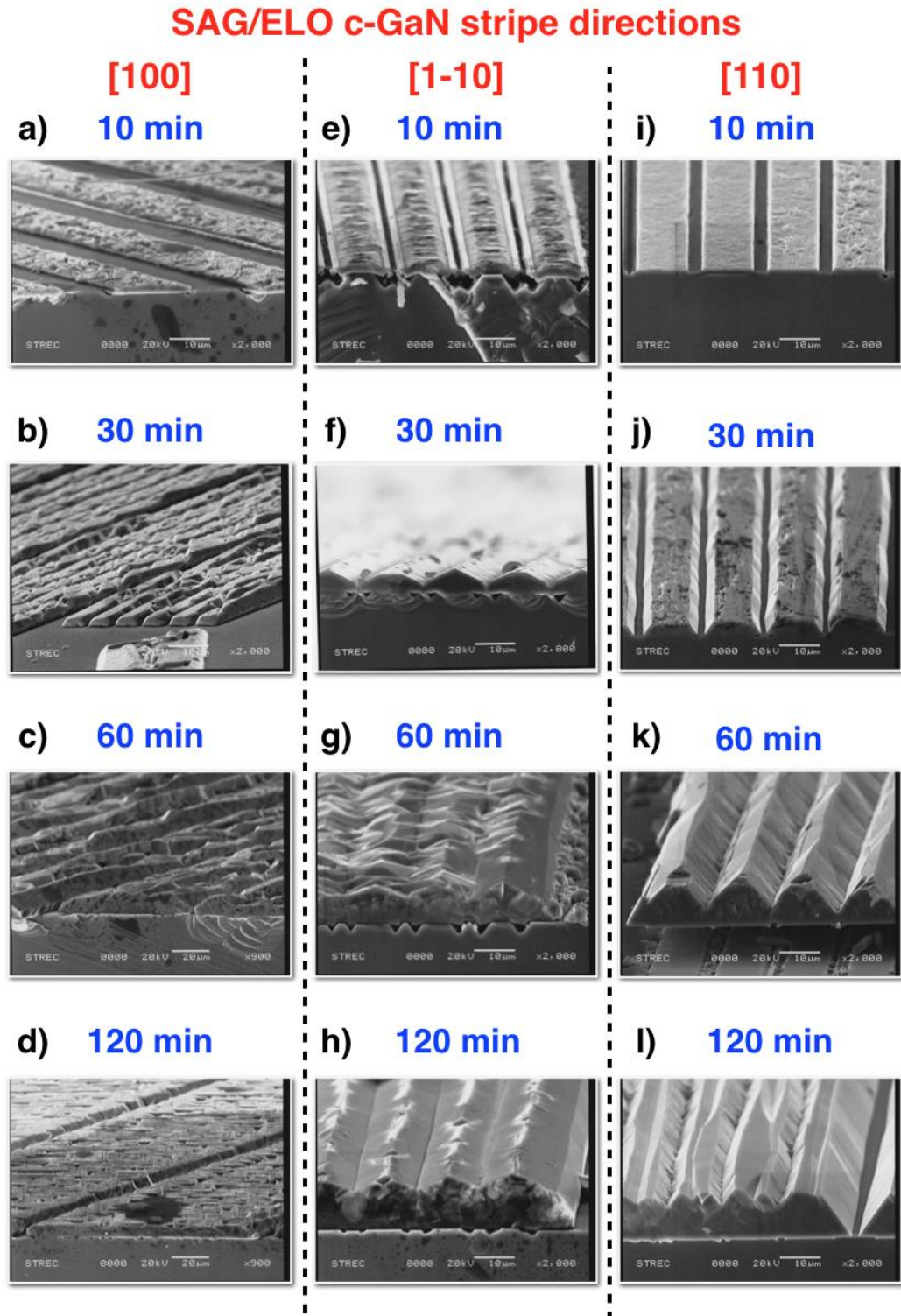


Figure 4.4: Cross-sectional view SEM images of SAG/ELO c-GaN on (a-d) [100], (e-h) [1-10] and (i-l) [110] mask pattern GaAs (001) at the growth time of 10 to 120 min.

On the [1-10] mask direction, as shown in Fig. 4.4 (e-h). The average thickness of SAG/ELO is  $\sim 2.3 \mu\text{m}$  at the growth time of 10 minutes and SAG/ELO c-GaN films have the (001) top rough facets and the dominant (113) sidewall facets with small (111) sidewall facets at the edge of SAG/ELO c-GaN stripe films. The (113) sidewall facets appear smooth facets with small (111) sidewall facet on the mask area at the growth time of 30 minutes, as shown in Fig. 4.4 (f). The shape of SAG/ELO c-GaN stripe film is the triangle shape with (113) sidewall facets and the highest thickness is  $\sim 9.7 \mu\text{m}$ , as shown in Fig. 4.5 (a). The angle between (001) facet and (113) facet around  $25.24^\circ$ .

The lateral growth rate is higher than vertical growth rate during at the growth time of 60 to 120 minutes which the thickness of the SAG/ELO c-GaN films on the mask area are increasing more than on the windows area. The SAG/ELO c-GaN films have rough surface (113) sidewall facets at the growth time of 60 minutes while the smooth (113) sidewall facets are appeared at the growth time of 120 minutes. On the [110] direction, as shown in Fig 4.4 (i-l), SAG/ELO c-GaN films have nearly smooth surface on (001) plane with the average thicknesses is 1.4 and  $3.5 \mu\text{m}$  at the growth time of 10 and 30 minutes, respectively. The trapezoidal shape is shown at the growth time of 30 minutes with (111) sidewall facet. The SAG/ELO c-GaN films are changed to triangle shape at the growth time of 60 minutes with (111) sidewall facet which the thickness is  $\sim 12 \mu\text{m}$ . At the growth time of 120 minutes, as shown in Fig. 4.5 (b), SAG/ELO c-GaN films are clearly observed with smooth (111) sidewall facets with top flat (001) facet. The angle between (001) facet and (111) facet around  $54.73^\circ$ .

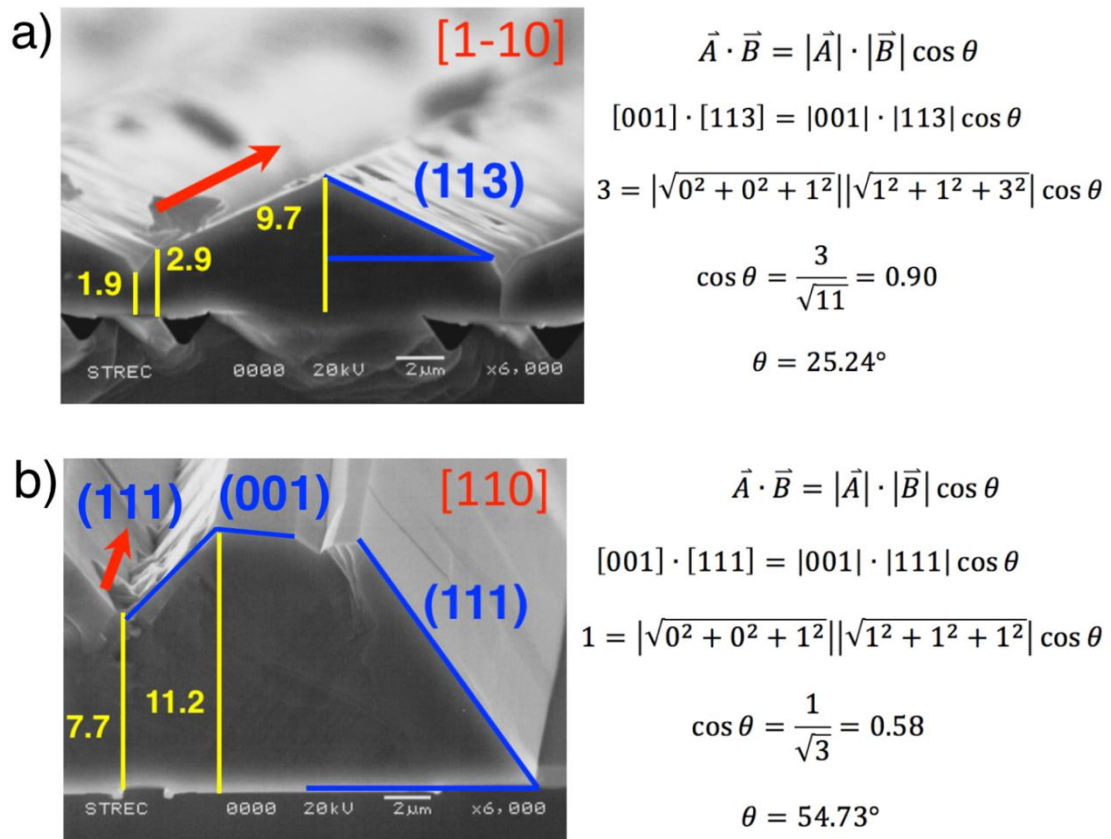


Figure 4.5: Cross-sectional view of SEM images (x6000) of ELO c-GaN on GaAs (001) a) [1-10] at growth time of 30 min and b) [110] at growth time of 120 min.

In Table 4.1, the vertical growth rate show that the morphologies of SAG/ELO c-GaN on (001) plane has higher vertical growth rate than (111) and (113) planes. The SAG/ELO c-GaN on [100] mask stripe direction has the highest vertical growth rate during at the growth time of 30 to 60 minutes.

Table 4.1: The vertical growth rate of SAG/ELO c-GaN on [100], [1-10] and [110] mask patterned GaAs (001)

Mask Pattern	Growth Time			
	0-10 min	10-30 min	30-60 min	60-120 min
[100]	0.180	0.010	0.306	-
[1-10]	0.230	0.165	0.113	0.043
[110]	0.140	0.105	0.283	-

### 4.3 Micro Raman Scattering Spectroscopy

The spotted areas of  $\sim 2 \mu\text{m}$  in size are shown in Fig. 4.6. The specific area on the top surface and sidewall facet of SAG/ELO c-GaN films for [100], [1-10] and [110] mask stripe directions at the growth time of 10 to 120 minutes are investigated to identify the cubic and hexagonal GaN structures from the phonon vibrational in TO and LO modes. Some of data do not appear on the Raman intensity graphs because of the Raman intensities of GaAs in TO and LO modes are not shown.

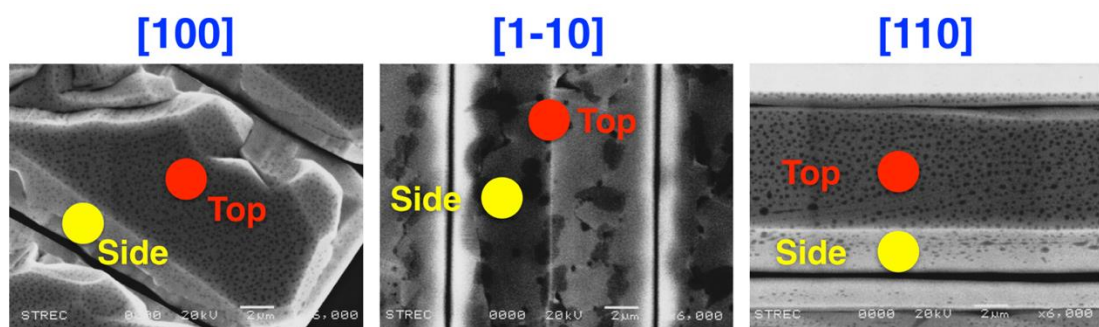


Figure 4.6: Micro Raman spot size  $\sim 2 \mu\text{m}$  on the top and side facets of SAG/ELO c-GaN films.

The phonon vibrational modes of cubic and hexagonal GaN structures are shown in Fig. 4.7. The phonon mode of c-GaN structure has the dominant peak intensity at c-GaN (LO) with Raman shift at  $738\text{ cm}^{-1}$  while the phonon modes of h-GaN are shown at h-GaN  $A_1$  (TO), h-GaN  $E_1$  (TO) and h-GaN  $E_2$  (high) with Raman shift at  $533, 558, 568\text{ cm}^{-1}$ , in agreement [32].

The Raman spectra graphs are normalized with GaAs (LO) and (TO) intensities, as shown in Fig. 4.8. Only the phonon vibrational mode of h-GaN  $A_1$  (TO) with Raman shift at  $538\text{ cm}^{-1}$  for SAG/ELO c-GaN on the mask stripe pattern [1-10] GaAs (001) is different from the others. On the [100] direction, as shown in Fig. 4.8 (a-b), the high intensity of h-GaN  $E_2$  (high) appears at the top facet while the sidewall facet, the h-GaN  $A_1$ (TO) appears at higher than h-GaN  $E_2$  (high). The result of high Raman intensity of h-GaN is the structure of SAG/ELO c-GaN films which has the top rough surface with unclear sidewall facets. High intensity of c-GaN (LO) is observed on the [1-10] mask stripe direction especially at the (113) sidewall facet, as shown in Fig. 4.8 (d). The Raman intensity of c-GaN (LO) is higher than  $E_2$  (high) at the growth time of 60 minutes which the morphology of the (113) sidewall facets are rough surface from high lateral growth rate. Raman intensities at the top of c-GaN on [110] mask stripe direction, as shown in Fig. 4.8 (e), show high h-GaN  $E_2$  (high). The crack lines along to [110] mask stripe direction on the top surface have clearly appeared at the growth time of 120 minutes. These planes along crack lines might be the plane to generate cubic phase GaN. The (111) sidewall facet where is the hexagonal phase inclusion can generate. At the growth time of 120 minutes on the sidewall facet, the Raman intensity of c-GaN (LO) is very low compare with h-GaN

$E_2$  (high). However, Raman spectra measured from the spot size area which does not give the information of the whole sample.

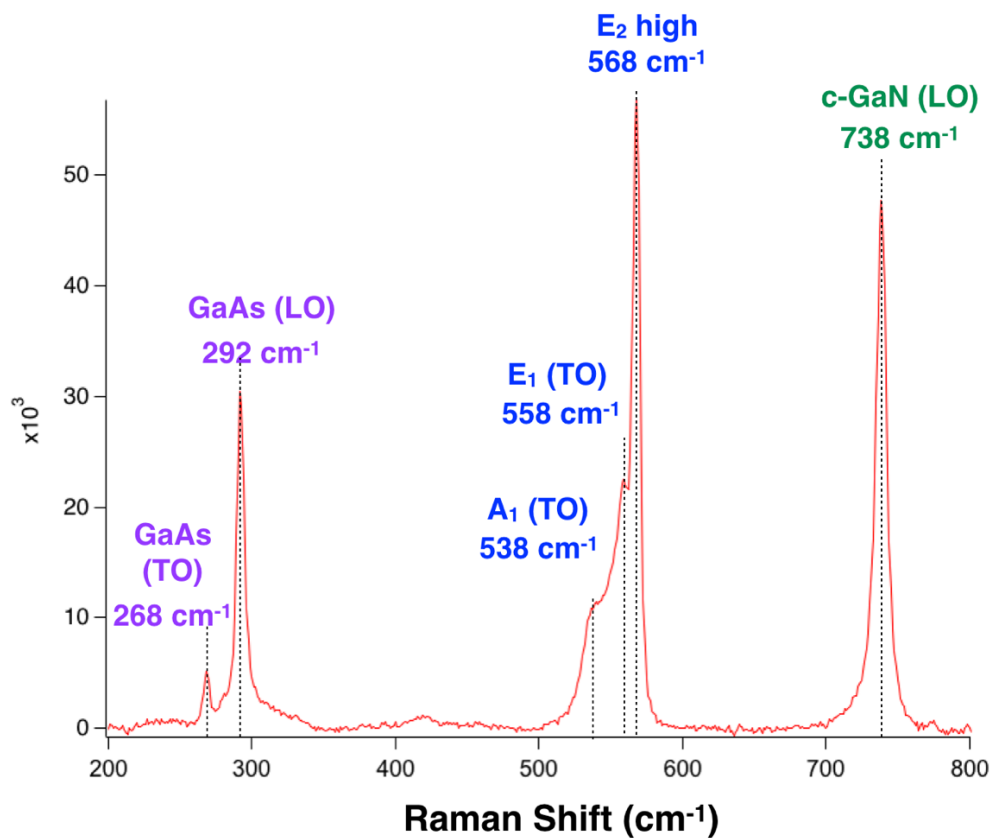


Figure 4.7: Raman spectra on the top area of SAG/ELO c-GaN on [1-10] mask patterned GaAs (001) at growth time of 120 minutes.

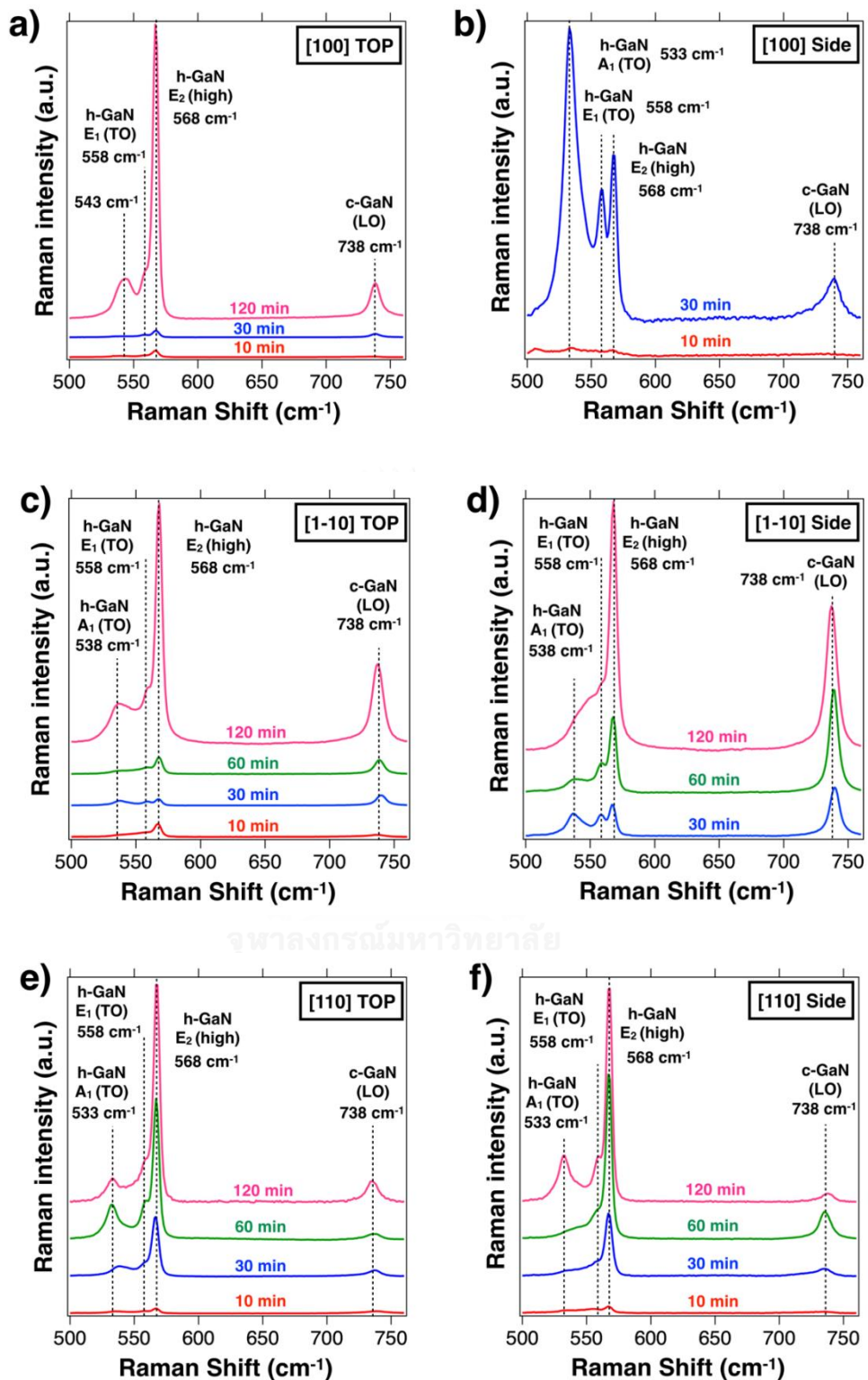


Figure 4.8: Raman spectra of ELO c-GaN on GaAs (001) on the top and sidewall facets with different growth times and mask stripe directions.

## 4.4 High Resolution X-ray Diffraction

HRXRD was operated in  $2\theta/\omega$ -scan,  $\Delta(2\theta/\omega)$ , rocking curve ( $\omega$ -scan) and reciprocal space mapping (RSM) modes.

### 4.4.1 $2\theta/\omega$ -scan Profiles

HRXRD  $2\theta/\omega$ -scan profiles of ELO c-GaN on GaAs (001) are measured in the range of 31 to 41 degrees. As shown in Fig. 4.9, the graphs are divided with mask stripe directions. The GaAs (002) X-ray intensities are normalized to compare the c-GaN (002). The  $2\theta/\omega$ -scan profiles of SAG/ELO c-GaN on [100] mask stripe direction shows small peaks of h-GaN (0002)  $34.56^\circ$  and h-GaN (10-11)  $36.58^\circ$  at the growth time of 60 and 120 minutes. The Normalized FWHM  $\Delta(2\theta/\omega)$  profiles of c-GaN (002) are 9.03, 6.66, 5.39 and 4.54 arcmin, respectively. When the growth time are increased, the FWHM  $\Delta(2\theta/\omega)$  profiles of c-GaN (002) are decreased which means that the SAG/ELO c-GaN films are relaxation. The X-ray intensities of h-GaN (0002) and h-GaN (10-11) are clearly observed on the [1-10] mask stripe directions by comparing with others. The FWHM  $\Delta(2\theta/\omega)$  profiles of c-GaN (002) are decreased from 12.15 to 5.25 arcmin at longer growth time of 10 to 120 minutes. On [100] mask stripe direction, the  $2\theta/\omega$ -scan profiles of SAG/ELO c-GaN have not shown any X-ray intensities of h-GaN (0002) and h-GaN (10-11). At the growth time of 60 minutes, the FWHM  $\Delta(2\theta/\omega)$  profile of c-GaN (002) is 4.92 arcmin which lower than 5.96 arcmin at the growth time of 120 minutes.

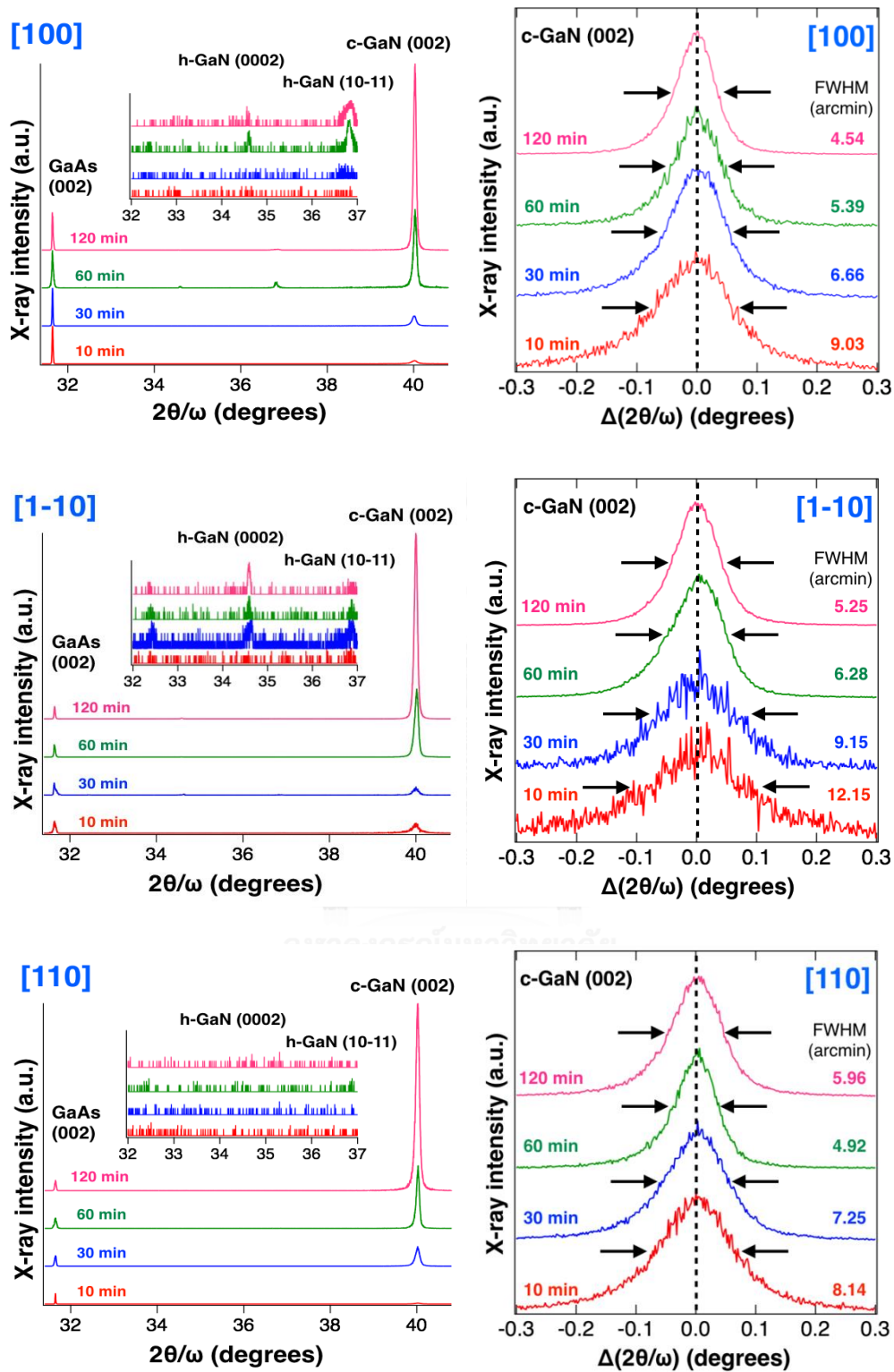


Figure 4.9: HRXRD  $2\theta/\omega$ -scan profiles of SAG/ELO c-GaN on [100], [1-10] and [110] mask stripe patterned GaAs (001) and normalized FWHM  $\Delta(2\theta/\omega)$  profiles of c-GaN (002).

#### 4.4.2 Rocking Curve

The crystal orientation of c-GaN (002) is measured with X-ray incident beam direction perpendicular and parallel to the mask stripe directions. The quality of the films depends on the mosaic in the c-GaN films, which is measured by FWHM of X-ray rocking curve. It is known that the narrower FWHM show better quality.

In Fig. 4.10, the FWHM is decreased during at the growth time of 10 minutes to 30 minutes which is the vertical growth rate higher than lateral growth rate. The FWHM is also decreased during at the growth time of 60 to 120 minutes which the lateral growth rate higher than vertical growth rate. While at the growth time of 30 to 60 minutes, the FWHM are increased except FWHM of [1-10] with X-ray incident beam perpendicular direction.

The  $\omega$ -scan profiles of c-GaN (002) with incident X-ray beam perpendicular and parallel are shown in Fig. 4.11. At the growth time of 30 minutes, the high vertical growth rate shows lower FWHM of c-GaN (002) than the lower vertical growth rate at the growth time of 10 minutes. While at the growth time of 120 minutes, the lower lateral growth rate shows better result of FWHM of c-GaN (002) than the higher lateral growth rate at the growth time of 60 minutes. During the growth time of 30 to 60 minutes, the FWHM of c-GaN (002) are increased due to the changing from major direction of the growth rate of vertical and lateral.

The previous experiment was reported FWHM around 31 arcmin with the high cubic phase purity more than 85% for SAG c-GaN on GaAs (100) by MOVPE [26]. Our results of FWHM of SAG/ELO c-GaN on GaAs (001) have lower 27 arcmin.

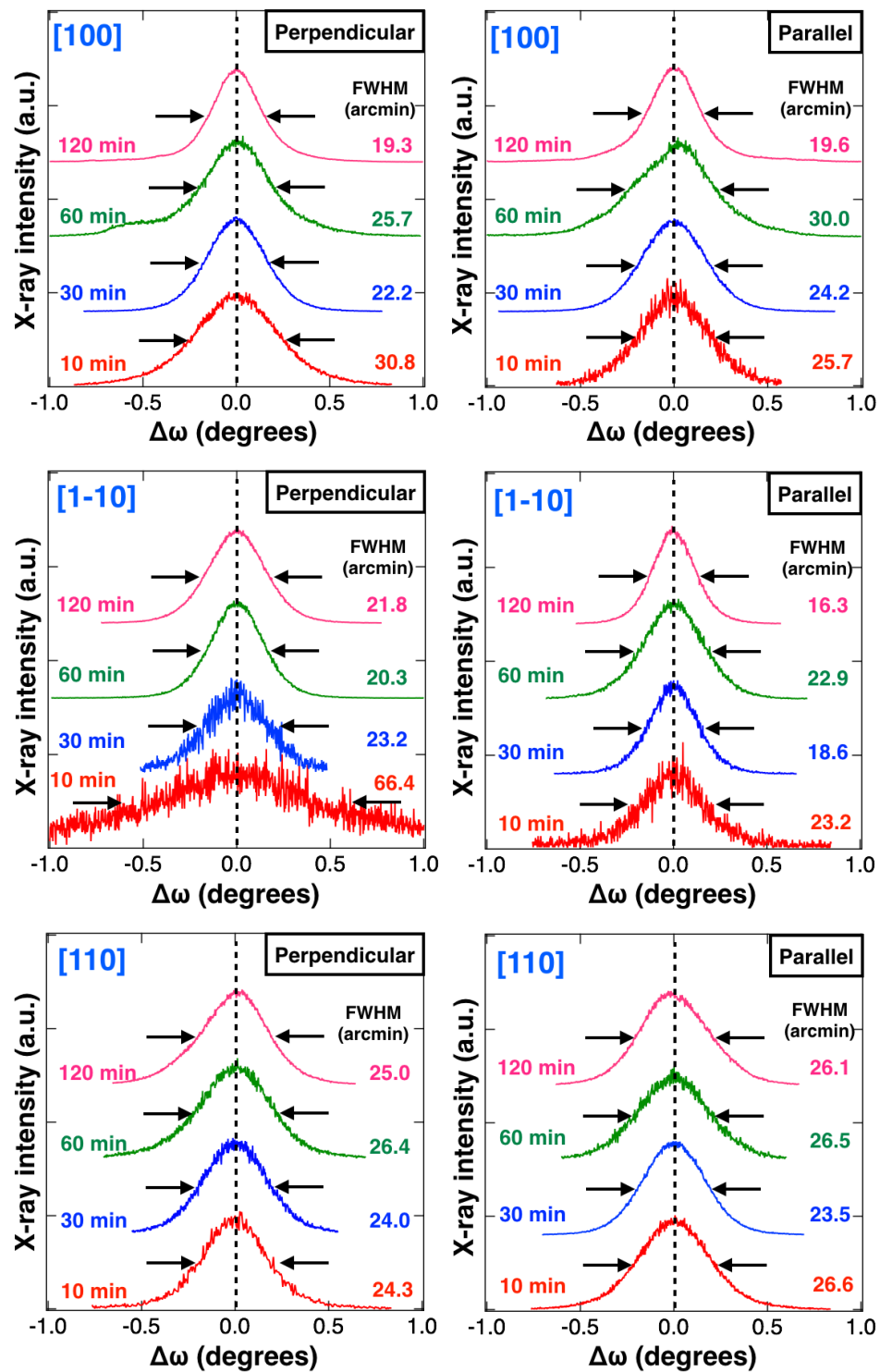


Figure 4.10: HRXRD c-GaN (002)  $\omega$ -scan profiles of incident X-ray directions perpendicular and parallel with [100], [1-10] and [110] mask stripe directions.

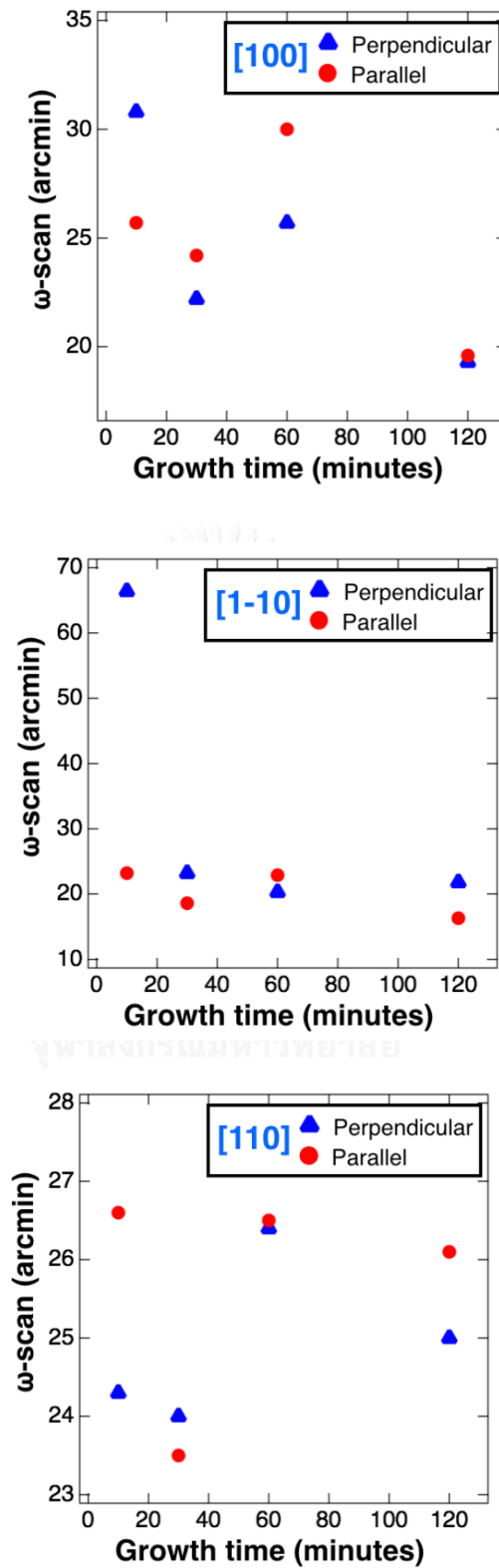


Figure 4.11:  $\omega$ -scan profiles of incident X-ray perpendicular and parallel to [100], [1-10] and [110] mask stripe directions at growth time of 10 to 120 min.

### 4.4.3 Reciprocal Space Mapping

Symmetrical RSM of c-GaN (002) has the highest intensity c-GaN (002) around  $40^\circ$  and h-GaN {10-11} has found at  $\Delta\omega$  around  $-7$  and  $7^\circ$ . For each mask stripe direction, the X-ray intensities of c-GaN (002) were normalized with the same growth time for incident X-ray beam direction perpendicular and parallel with mask stripe pattern. As shown in Fig. 4.12, the lowest integrated X-ray intensities of hexagonal phase inclusion ( $V_h$ ) has 17.5% at the growth time of 30 minutes, which h-GaN {10-11} have the lowest X-ray intensities compare with other growth times. The hexagonal phase inclusion has the highest 58.8% at the growth time of 120 minutes.

The X-ray intensities of h-GaN {10-11} have higher than c-GaN (002) at the growth time of 10 and 20 minutes for ELO c-GaN on [1-10] mask stripe directions which the integrated X-ray intensities of hexagonal phase inclusion are higher than 80%, as shown in Fig. 4.13. Although, X-ray intensities of h-GaN {10-11} are low at the growth time of 60 minutes with X-ray incident beam parallel direction and 120 minutes with X-ray incident beam perpendicular with [1-10] mask stripe direction, but the hexagonal phase inclusion still more than 50%.

The X-ray incident beam direction perpendicular to [110] mask stripe direction shows the higher h-GaN {10-11} intensities than X-ray beam direction parallel to [110] mask stripe direction for all growth time, as shown in Fig. 4.14. At the growth time of 60 minute that the h-GaN {10-11} have higher X-ray intensities than c-GaN (002) which the hexagonal phase inclusion is 91.2%. The lowest hexagonal phase inclusion is 2.6% which nearly no X-ray intensities of h-GaN {10-11} at the growth time of 30 minutes.

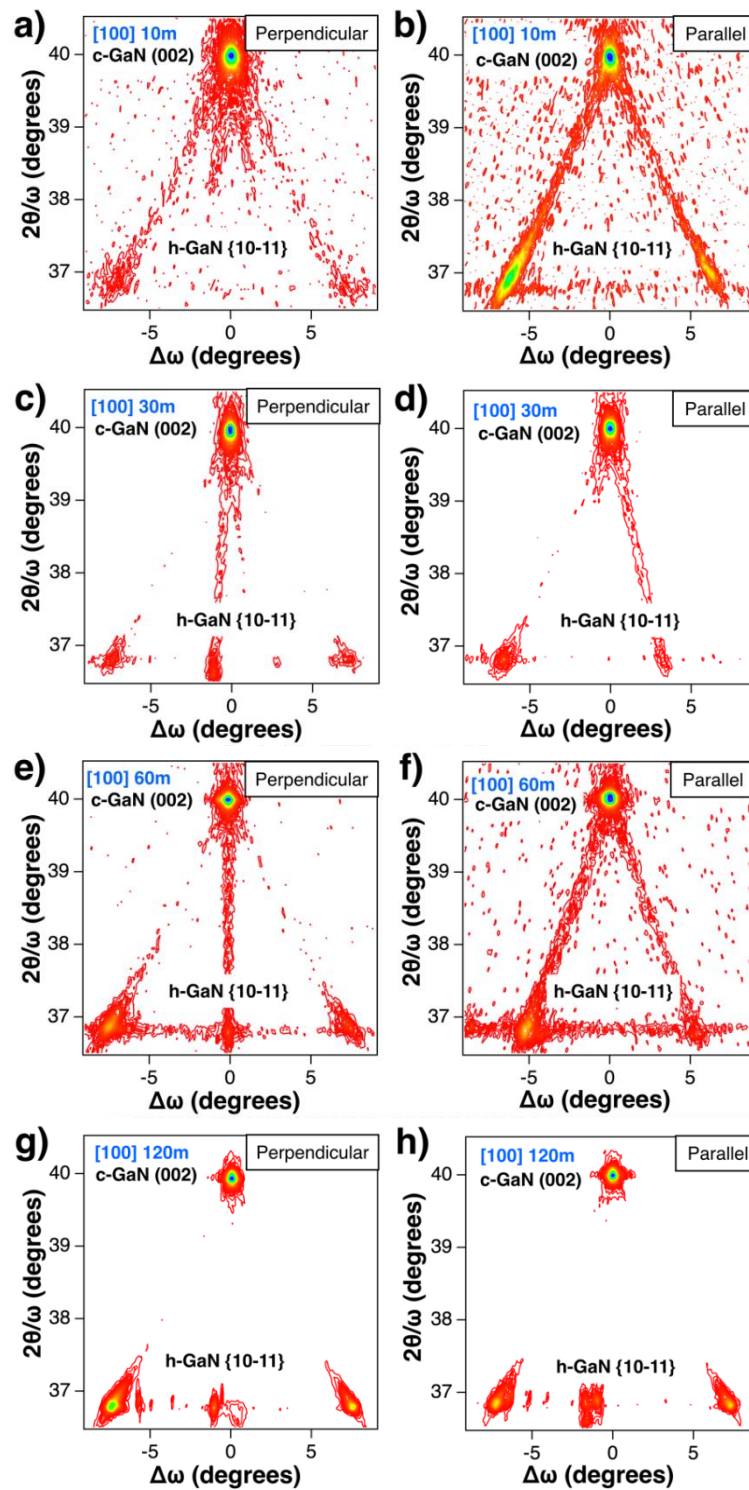


Figure 4.12: Symmetrical RSMs of c-GaN (002) for [100] mask stripe pattern with normalized c-GaN (002) individual growth times.

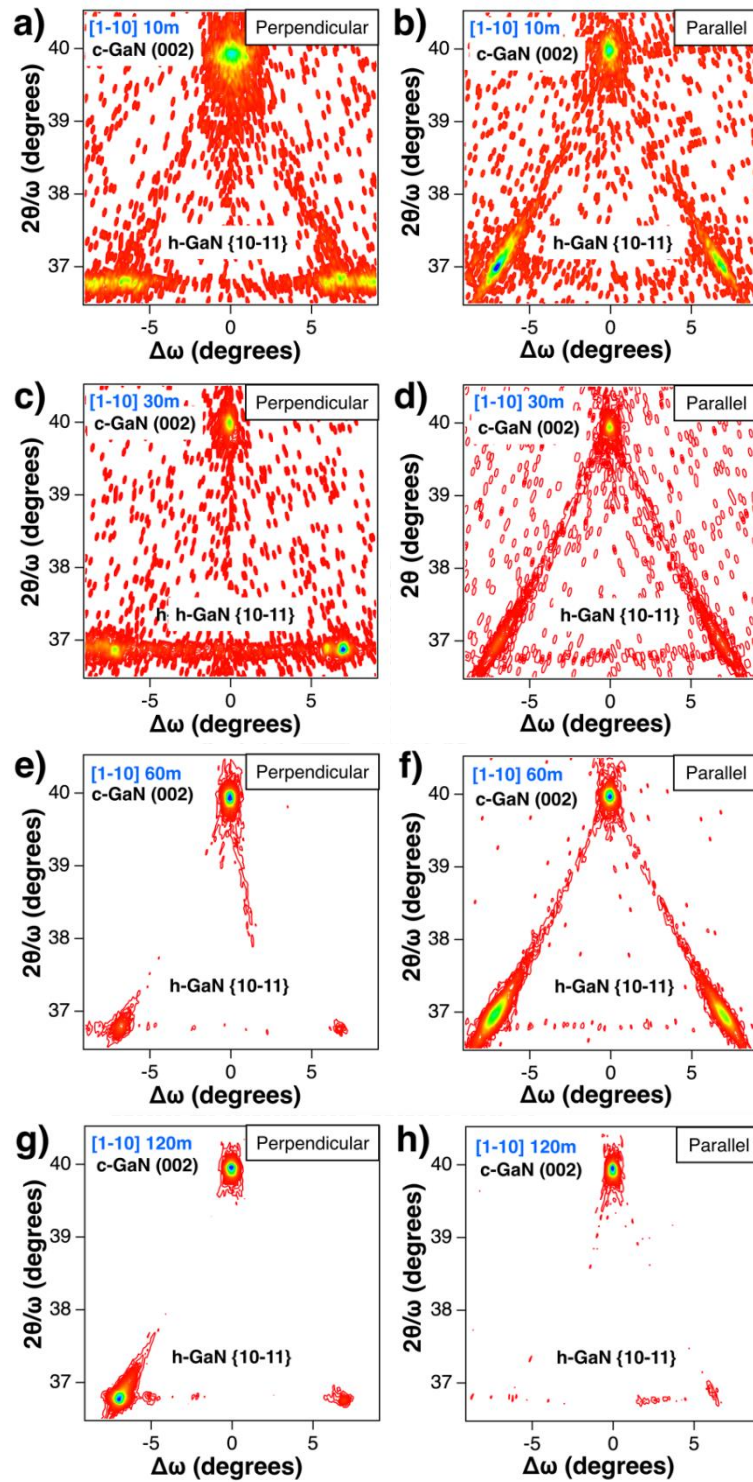


Figure 4.13: Symmetrical RSMs of c-GaN (002) for [1-10] mask stripe pattern with normalized c-GaN (002) individual growth times.

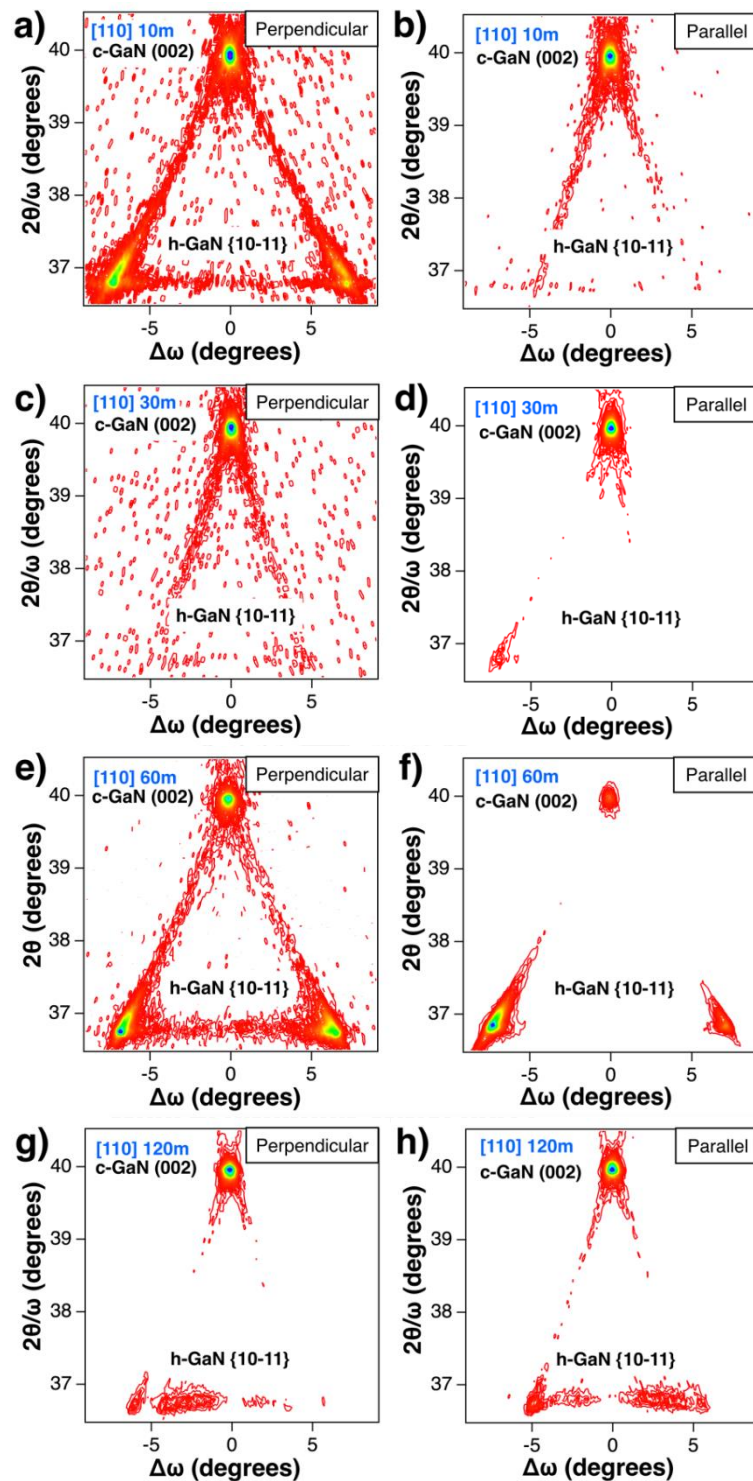


Figure 4.14: Symmetrical RSMs of c-GaN (002) for [110] mask stripe pattern with normalized c-GaN (002) individual growth times.

Table 4.2: The growth time with the integrated intensities of hexagonal phase inclusion.

	Growth Time	2 $\theta$ of c-GaN (002)	Lattice Constant c-GaN	Strain (%) $\Delta a/a$	%Vh (error ~1%)
<b>[100]</b>	10	40.015	4.503	0.005	45.3
	30	40.010	4.503	-0.007	<b>17.5</b>
	60	40.033	4.501	0.048	33.2
	120	40.028	4.501	0.036	58.8
<b>[1-10]</b>	10	39.988	4.506	-0.060	80.5
	30	39.996	4.505	-0.041	85.4
	60	40.014	4.503	0.002	59.3
	120	39.999	4.505	-0.034	<b>57.0</b>
<b>[110]</b>	10	40.021	4.502	0.019	49.7
	30	40.017	4.503	0.009	<b>2.6</b>
	60	40.025	4.502	0.029	91.2
	120	40.018	4.502	0.012	15.4

In Table 4.2, the strain which are calculated from 2 $\theta$  of c-GaN (002) from 2 $\theta/\omega$ -scan mode and the summarize of the integrated X-ray intensities of hexagonal phase inclusion. The strain in ELO c-GaN is calculated from 2 $\theta/\omega$ -scan at the 2 $\theta$  of c-GaN (002) position. The strain has positive value is compressive strain while negative is tensile strain.

SAG/ELO c-GaN on [100] mask stripe pattern GaAs (001) has the lowest hexagonal phase inclusion at the growth time of 30 minutes. The SEM image, as shown in Fig. 4.4 (b), show that the SAG/ELO c-GaN stripe films are grown on windows area without merging on the mask area. While the SAG/ELO c-GaN films are merge on the mask area, the hexagonal phase inclusion is increasing from 33.2% to 58.8% at growth time of 60 and 120 minutes, respectively. The result of SEM images shows the top rough surface which is not good to do the continue process for applications.

On the [1-10] mask stripe direction, the hexagonal phase inclusion is reduced from ~80% to ~50% at the growth time of 10 to 120 minutes. The reducing of hexagonal phase inclusion because the (111) sidewall facets at the edge of c-GaN stripe films are limited on the mask area under dominated (113) sidewall facets, as shown in Fig. 4.4 (g-h). The (113) sidewall facets are the plane that c-GaN structure is dominated. The Raman spectra also confirm that (113) sidewall facet is the plane that has c-GaN structure higher than h-GaN structure, as shown in Fig. 4.15 (a). The Raman intensities ratio of c-GaN (LO) to c-GaN (LO) with h-GaN E<sub>2</sub> high are shown at the growth time of 10 to 120 minutes, as shown in Fig. 4.15 (b). The highest intensities appear at growth time of 30 minute which (111) sidewall facets can be observe at the edge of c-GaN stripes.

On the [110] mask stripe direction, the lowest hexagonal phase inclusion is 2.6% at the growth time of 30 minutes. From SEM images, the SAG/ELO c-GaN films has the top flat facet with (111) sidewall facet, as shown in Fig. 4.4 (j). The integrated X-ray intensities of h-GaN {10-11} has the highest value at the growth time of 60 minutes which the growth morphologies from SEM images show triangle

shape with (111) sidewall facet, as shown in Fig. 4.4 (k). From the growth morphologies and hexagonal phase inclusion on [110] mask stripe direction, the high cubic phase GaN is related to (001) flat facet on the top of SAG/ELO c-GaN films, as shown in Fig. 4.16 (b).

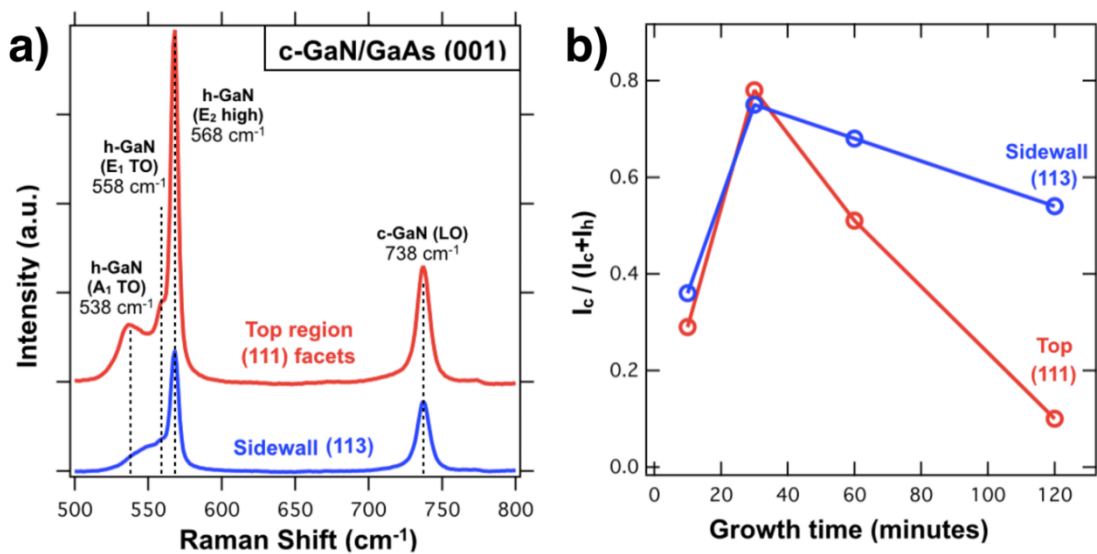


Figure 4.15: (a) Raman spectra of c-GaN stripe on the top and sidewall facets and (b) Integrated Raman intensities ratio of c-GaN (LO) to c-GaN (LO) with h-GaN E<sub>2</sub> high.

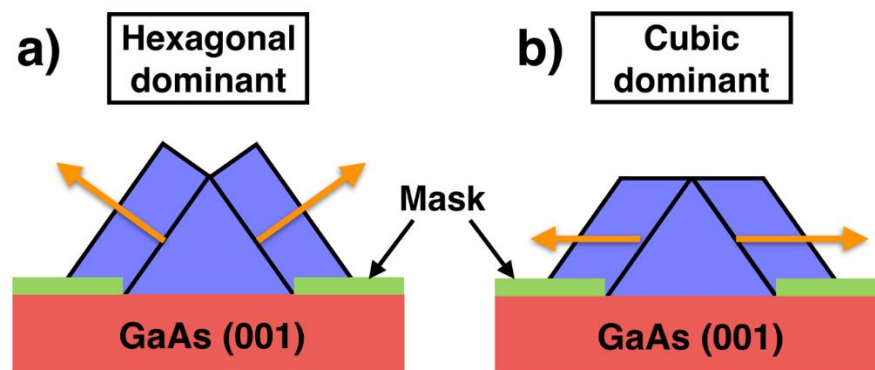


Figure 4.16: Morphologies of ELO c-GaN on [110] mask stripe pattern GaAs (001) (a) with h-GaN dominant and (b) with c-GaN dominant.

## CHAPTER V

### CONCLUSIONS

High quality cubic phase GaN films were grown by selective area growth and epitaxial lateral overgrown methods. The c-GaN films were grown on [100], [1-10] and [110] mask stripe patterned GaAs (001) substrates by metalorganic vapor phase epitaxy. Double buffer layers of GaAs and low temperature GaN were grown before c-GaN films. The growth temperature of c-GaN was 900 °C with steady pressure of 160 Torr in horizontal reactor to obtain high cubic phase purity. In this dissertation, the c-GaN films were grown at the growth time of 10, 30, 60 and 120 minutes to observe growth morphologies and crystal phase transformation from the growth time evolution.

Summary of the growth time evolution is as follows;

(i) The [100] mask stripe direction: The SEM images showed that the ELO c-GaN films were merged together on mask oxide at the growth time of 30 minutes with no sidewall facets. The rough surface appears with large cracks. The larger cracks were observed on the surface. The result of Raman spectra shows high intensities of h-GaN E2 (high) on the top surface and A1 (TO) sidewall facets. The hexagonal phase inclusion was increased with increasing growth time after the ELO c-GaN films were merged.

(ii) The [1-10] mask stripe direction: The ELO c-GaN films had (113) sidewall facets with small (111) sidewall facets at the edges of the ELO c-GaN Stripe films. The large amount of hexagonal phase inclusion was observed at the growth times of

10 and 30 minutes where the (111) sidewall facets are clearly observed. While at the growth times of 60 and 120 minutes, the hexagonal phase inclusion decreased which was related to (111) sidewall facet is limited under (113) sidewall facets. The Raman spectra showed high c-GaN (LO) at the (113) sidewall facet. However, the hexagonal phase inclusion was still higher value than other mask stripe directions. Although the hexagonal phase inclusion is decreased at the longer growth time. This was resulted from mask fill factor which was not suitable to grow ELO c-GaN films.

(iii) The [110] mask stripe direction: The (111) sidewall facets were clearly observed at the growth times of 30 to 120 minutes. The lowest hexagonal phase inclusion is 2.6% when the (111) sidewall facets were generated at the growth time of 30 minutes. The mask fill factor is also an important factor especially on this mask stripe direction. The mask fill factor 0.76 was found to be the most suitable value to grow high cubic phase purity of ELO GaN on GaAs (001).

From our result, the high cubic phase purity of ELO GaN films on GaAs (001) could be obtained on both the [1-10] and [110] mask stripe directions. For ELO c-GaN with [110] mask stripe direction, the cubic phase is remained when the (001) surface is kept during the growth. On the other hand, for [1-10] mask stripe direction, cubic phase is dominant, when the (113) surface is stable.

## REFERENCES

- [1] Yoshida, S. Growth of cubic III-nitride semiconductors for electronics and optoelectronics application. Physica E. 7 (2000) : 907-14.
- [2] Wu, J.Q. When group-III nitrides go infrared: New properties and perspectives. J Appl Phys. 106 (2009) : 011101-1-28.
- [3] Kong, J., and others. Optical properties of InN films grown by MOCVD. Front Optoelectron China. 1(2008) : 341-4.
- [4] Bai, J., Yang, C.C., Athanasiou, M., and Wang, T. Efficiency enhancement of InGaN/GaN solar cells with nanostructures. Appl Phys Lett. 104 (2014) : 051129.
- [5] Takagi, S., and others. High-Power (over 100 mW) Green Laser Diodes on Semipolar {20(2)over-bar1} GaN Substrates Operating at Wavelengths beyond 530 nm. Appl Phys Express. 5 (2012) : 082102-1-3.
- [6] Amano, H., Kito, M., Hiramatsu, K., and Akasaki, I. P-Type Conduction in Mg-Doped GaN Treated with Low-Energy Electron Beam Irradiation (LEEBI). Jpn J Appl Phys. 28 (1989) : L2122-L-14.
- [7] Nakamura, S., Senoh, N., Iwasa, N., and Nagahama, S.I. High-Brightness InGaN Blue, Green and Yellow Light-Emitting-Diodes with Quantum-Well Structures. Jpn J Appl Phys. 34 (1995) : L797-L9.
- [8] Onabe, K., and others. Cubic III-nitrides: potential photonic materials. Proc SPIE 7945 Quantum Sensing and Nanophotonic Devices VIII. 794517 (2011) : 1-8.
- [9] Park, S.H. Effect of Modulation Doping on the Spontaneous Emission Characteristics of Wurtzite GaN/AlGaIn Quantum Well Structures. J Korean Phys Soc. 55 (2009) : 2522-7.

- [10] Jung, Y., Mastro, M., Hite, J., Eddy, C.R., and Kim, J. Electrical and structural characterizations of non-polar AlGa<sub>N</sub>/Ga<sub>N</sub> heterostructures. Thin Solid Films. 518 (2010) : 1747-50.
- [11] Paskova, T., and others. Nonpolar a- and m-plane bulk Ga<sub>N</sub> sliced from boules: structural and optical characteristics. Phys Status Solidi C. 4 (2007) : 2536-9.
- [12] Kukushkin, S.A., Osipov, A.V., Bessolov, V.N., Medvedev, B.K., Nevolin, V.K., and Tcarik, K.A. Substrates for epitaxy of gallium nitride: New materials and techniques. Rev Adv Mater Sci. 17 (2008) : 1-32.
- [13] Hiramatsu, K. Epitaxial lateral overgrowth techniques used in group III nitride epitaxy. J Phys-Condens Mat. 13 (2001) : 6961-75.
- [14] Suandon, S., Sanorpim, S., Yoodee, K., and Onabe, K. Effect of growth temperature on polytype transition of Ga<sub>N</sub> from zincblende to wurtzite. Thin Solid Films. 515 (2007) : 4393-6.
- [15] Kuwano, N., and others. Formation of Cubic Ga<sub>N</sub> on (111)B Ga<sub>As</sub> by Metal-Organic Vapor-Phase Epitaxy with Dimethylhydrazine. Jpn J Appl Phys. 33 (1994) : 3415-6.
- [16] Hong, C.H., Wang, K., and Pavlidis, D. Epitaxial-Growth of Cubic Ga<sub>N</sub> on (111)Ga<sub>As</sub> by Metalorganic Chemical-Vapor-Deposition. J Electron Mater. 24 (1995) : 213-8.
- [17] Sanorpim, S., Discharoen, N., and Onabe, K. Cubic Ga<sub>N</sub> Growth on (311)A Ga<sub>As</sub> substrate by MOVPE. Phys Status Solidi C. 7 (2010) : 2076-8.
- [18] Chen, H., and others. Controllable cubic and hexagonal Ga<sub>N</sub> growth on Ga<sub>As</sub>(001) substrates by molecular beam epitaxy. J Cryst Growth. 210 (2000) : 811-4.

- [19] Kimura, R., and Takahashi, K. Investigation of the initial growth of cubic-GaN using an AlGaAs buffer layer grown on GaAs (100) by molecular beam epitaxy. J Cryst Growth. 227 (2001) : 395-8.
- [20] Liu, H.F., Chen, H., Wan, L., Li, Z.Q., Huang, Q., and Zhou, J.M. Epitaxial growth and characterization of GaN Films on (001) GaAs substrates by radio-frequency molecular beam epitaxy. J Cryst Growth. 227 (2001) : 390-4.
- [21] Parinyataramas, J., Sanorpim, S., Thanachayanont, C., and Onabe, K. Effect of AlGaAs Buffer Layer on Defect Distribution in Cubic GaN Grown on GaAs (001) by MOVPE. Chiang Mai J Sci. 40 (2013) : 971-7.
- [22] Wu, J., Zhao, F.H., Onabe, K., and Shiraki, Y. Metalorganic vapor-phase epitaxy of cubic GaN on GaAs (100) substrates by inserting an intermediate protection layer. J Cryst Growth. 221 (2000) : 276-9.
- [23] Shen, X.M., and others. X-ray diffraction analysis of MOCVD grown GaN buffer layers on GaAs(001) substrates. J Cryst Growth. 254 (2003) : 23-7.
- [24] Sormunen, J., Toivonen, J., Sopanen, M., and Lipsanen, H. Morphology of ultra-thin cubic GaN layers on GaAs(100) grown by MOVPE with DMHy as nitrogen source. Appl Surf Sci. 222 (2004) : 286-92.
- [25] Shen, X.M., and others. Structural characterization of epitaxial lateral overgrown GaN on patterned GaN/GaAs(001) substrates. J Cryst Growth. 246 (2002) : 69-72.
- [26] Fu, Y., and others. Epitaxial lateral overgrowth of cubic GaN by metalorganic chemical vapor deposition. J Cryst Growth. 225 (2001) : 45-9.

- [27] Sanorpim, S., Wu, J., Onabe, K., and Shiraki, Y. Effects of growth temperature in selective-area growth of cubic GaN on GaAs (100) by MOVPE. J Cryst Growth. 237 (2002) : 1124-8.
- [28] Sanorpim, S., Takuma, E., Katayama, R., Onabe, K., Ichinose, H., and Shiraki, Y. Reduction of planar defect density in laterally overgrown cubic-GaN on patterned GaAs(001) substrates by MOVPE. Phys Status Solidi B. 234 (2002) : 840-4.
- [29] Sanorpim, S., Takuma, E., Onabe, K., Ichinose, H., and Shiraki, Y. Laterally overgrown GaN on patterned GaAs (001) substrates by MOVPE. Phys Status Solidi A. 192 (2002) : 446-52.
- [30] Sanorpim, S. Wu, J., Onabe, K., and Shiraki, Y. Detection and Analysis of Hexagonal Phase Generation in Selective-Area Growth of Cubic GaN by Metalorganic Vapor Phase Epitaxy. Proceeding of the International Workshop on Nitride Semiconductors (IPAP Conference Series 1). 1 (2000) : 89-92.
- [31] Sumnavadee, S., Sanorpim, S., Paosawat, B., and Onabe, K. Stacking Fault and Its Effect on c-GaN Epitaxial Growth on GaAs (001). Journal of Microscopy Society of Thailand. 24 (2010) : 136-9.
- [32] Liu, H.F., and others. MBE growth and Raman studies of cubic and hexagonal GaN films on (001)-oriented GaAs substrates. J Cryst Growth. 218 (2000) : 191-6.
- [33] Kemper, R.M., and others. Anti-phase domains in cubic GaN. J Appl Phys. 110 (2011) : 123512-1-5.
- [34] Tabata, A., and others. Comparative Raman studies of cubic and hexagonal GaN epitaxial layers. J Appl Phys. 79 (1996) : 4137-40.
- [35] Sung, L.W., Lin, H.H., and Chia, C.T. Cubic GaN grown on (001) GaAs substrate by RF plasma assisted gas source MBE. J Cryst Growth. 241 (2002) : 320-4.

- [36] Bulbul, M.M., Smith, S.R.P., Obradovic, B., Cheng, T.S., and Foxon, C.T. Raman spectroscopy of optical phonons as a probe of GaN epitaxial layer structural quality. Eur Phys J B. 14 (2000) : 423-9.
- [37] Hushur, A., Manghnani, M.H., and Narayan, J. Raman studies of GaN/sapphire thin film heterostructures. J Appl Phys. 106 (2009) : 054317-1-5.
- [38] Davydov, V.Y., and others. Phonon dispersion and Raman scattering in hexagonal GaN and AlN. Phys Rev B. 58 (1998) : 12899-907.
- [39] Tsuchiya, H., Sunaba, K., Yonemura, S., Suemasu, T., and Hasegawa, F. Cubic dominant GaN growth on (001)GaAs substrates by hydride vapor phase epitaxy. Jpn J Appl Phys. 36 (1997) : L1-L3.
- [40] Kuntharin, S., Yaguchi, H., Iwahashi, Y., Orihara, M., Hijakata, Y., and Yoshida, S. High Resolution X-ray Diffraction and Raman Scattering Studies of Cubic-phase InN Films Grown by MBE. Adv Mat Res. 55-57 (2008) : 773-6.



**APPENDIX**

จุฬาลงกรณ์มหาวิทยาลัย  
CHULALONGKORN UNIVERSITY

## APPENDIX A

### LIST OF ACRONYMS

GaN	Gallium Nitride
AlN	Aluminium Nitride
InN	Indium Nitride
LDs	Laser diodes
LEDs	Light-emitting diodes
MQW	Multiple-quantum well
BD	Blu-ray Disc
GaP	Gallium Phosphide
WLEDs	White light-emitting diodes
RGB	Red-Green-Blue
UV	Ultraviolet
MOCVD	Metal organic vapour phase deposition
LEEBI	Low-Energy Electron-Beam Irradiation
QW	Quantum Well
VB	Valance Band
CB	Conduction Band
QCSE	Quantum Confined Stark Effect
GaAs	Gallium Arsenide
TEC	Thermal Expansion Coefficient

3C-SiC	Zincblende Silicon Carbide
MOVPE	Metal Organic Vapor Phase Epitaxy
SAG	Selective-area growth
ELO	Epitaxial lateral overgrowth
SEM	Scanning Electron Microscopy
HRXRD	High Resolution X-ray Diffraction
TDs	Threading Dislocations
SFs	Stacking Faults
ED	Electron Diffraction
TEM	Transmission Electron Microscopy
SAD	Selected Area Diffraction
FWHM	Full-Width at Half Maximum
LT	Low Temperature
FACEL	Facet Lateral Epitaxial Lateral Overgrowth
FF	Mask Fill Factor
TMGa	Trimethylgallium
DMhy	1-1-demethylhydrazine
TBAs	Tertiarybutylarsine
RF	Radio Frequency
LO	Longitudinal Optical mode
TO	Transverse Optical mode

## APPENDIX B

### LIST OF PUBLICATION AND CONFERENCES

#### PUBLICATION:

1) **Suwanyangyaun, P.**, Sanorpim, S. and Onabe, K., Micro-Raman Investigation of Epitaxial Lateral Overgrown Cubic GaN on Patterned GaAs (001) with Different Mask Stripe Directions. *Advanced Materials Research*, 2013. 802: p. 164-168

#### CONFERENCES:

1) **Suwanyangyaun, P.**, Sanorpim, S. and Onabe, K., Effect of Growth Time at The Cubic Phase GaN on GaAs (001) with Different Mask Stripe Orientations by MOVPE Using Selective-area Method, *The Science Forum 2011*, Bangkok, Thailand, March 10-11, 2011. **(Oral presentation)**

2) **Suwanyangyaun, P.**, Sanorpim, S. and Onabe, K., Selective-area to epitaxial lateral overgrowth of cubic phase GaN on GaAs (001) by MOVPE with different mask stripe orientations, *Siam Physics Congress 2011 (SPC 2011)*, Pattaya, Thailand, March 23-26, 2011. **(Poster presentation)**

3) **Suwanyangyaun, P.**, Sanorpim, S. and Onabe, K., Lateral Overgrowth of Cubic GaN on [1-10]-Stripe Patterned GaAs (001) Substrates by MOVPE, *The 37th Congress on Science and Technology of Thailand (SST37)*, Bangkok, Thailand, October 10-12, 2011. **(Poster presentation)**

- 4) **Suwanyangyaun, P.**, Sanorpim, S. and Onabe, K., Cubic GaN Selective-Area Growth on Stripe Patterned GaAs (001) Substrates by MOVPE, *The Sixteenth International Conference on Metal Organic Vapor Phase Epitaxy (ICMOVPE-XVI)*, Busan, Korea, May 20-25, 2012. **(Poster presentation)**
- 5) **Suwanyangyaun, P.**, Sanorpim, S. and Onabe, K., Raman Spectroscopy of Selective Area Grown Cubic GaN on GaAs (001) by MOVPE, *7th International Conference on Materials Science and Technology (MSAT 7)*, Bangkok, Thailand, June 7-8, 2012. **(Oral presentation)**
- 6) **Suwanyangyaun, P.**, Sanorpim, S. and Onabe, K., Selective-area to Epitaxial Lateral Overgrowth of Cubic GaN on GaAs (001) by MOVPE with Different Mask Stripe Orientations, *International Union of Materials Research Societies - International Conference in Asia 2012 (IUMRS-ICA 2012)*, Busan, Korea, August 26-31, 2012. **(Poster presentation)**
- 7) **Suwanyangyaun, P.**, Sanorpim, S. and Onabe, K., High Resolution X-ray Diffraction Analysis of ELO Cubic GaN on Mask Stripe Patterned GaAs (001) by MOVPE, *Siam Physics Congress 2012 (SPC 2012)*, Phra nakhon Si Ayutthaya, Thailand, May 9-12, 2012. **(Poster presentation)**
- 8) **Suwanyangyaun, P.**, Sanorpim, S. and Onabe, K., Selective-area of Cubic GaN on Mask Stripe Patterned GaAs (001) by MOVPE, *The Science Forum 2012*, Bangkok, Thailand, April 19-20, 2012. **(Oral presentation)**
- 9) **Suwanyangyaun, P.**, Sanorpim, S. and Onabe, K., High Resolution X-ray Diffraction of Lateral Overgrown Cubic GaN on GaAs (001) by MOVPE, *The Science Forum 2013*, Bangkok, Thailand, March 14-15, 2013. **(Oral presentation)**

- 10) **Suwanyangyaun, P.**, Sanorpim, S. and Onabe, K., Micro-Raman Investigation of Epitaxial Lateral Overgrown Cubic GaN on Patterned GaAs (001) with Different Mask Stripe Directions, *International Conference on Engineering, Applied Sciences, and Technology (ICEAST 2013)*, Bangkok, Thailand, August 21-24, 2013. **(Oral presentation)**
- 11) **Suwanyangyaun, P.**, Sanorpim, S. and Onabe, K., ELO cubic GaN on [1-10] Mask-Stripe Patterned GaAs (001) by MOVPE, *Siam Physics Congress 2014 (SPC 2014)*, Nakhon Ratchasima, Thailand, March 26-29, 2014. **(Poster presentation)**
- 12) **Suwanyangyaun, P.**, Sanorpim, S. and Onabe, K., Crystal Structures of ELO Cubic GaN on [1-10] Mask Stripe Patterned GaAs (001) Substrates Grown by MOVPE, *17th International Conference on Metalorganic Vapor Phase Epitaxy (ICMOVPE XVII)*, Lausanne, Switzerland, July 13-18, 2014. **(Poster presentation)**
- 13) **Suwanyangyaun, P.**, Sanorpim, S. and Onabe, K., Crystal Structures of ELO Cubic GaN on [1-10] Mask Stripe Patterned GaAs (001) Grown by MOVPE, *Workshop - Nanoscience & Nanomedicine, Nanyang Technological University*, Singapore, September 11-12, 2014. **(Poster presentation)**
- 14) **Suwanyangyaun, P.**, Sanorpim, S. and Onabe, K., High-Quality Pure Cubic GaN on Patterned GaAs (001) Substrates with [110]-Oriented Stripes by MOVPE, *Siam Physics Congress 2015 (SPC 2015)*, Krabi, Thailand, May 20-22, 2015. **(Oral presentation)**

## VITA

Mr. Pattana Suwanyangyaun was born on May 13, 1978 in Bangkok, Thailand. Subsequent to receiving his Bachelor of Science in Physics from Chulalongkorn University, Bangkok, Thailand in 2000, he earned a Master of Engineering Science in Photovoltaic Engineering from The University of New South Wales, Australia in 2003. He entered Doctor of Philosophy in Nanoscience and Technology, Graduate School of Chulalongkorn University in 2011.

Currently, He has published one international scientific paper in Advanced Material Research. He has participated in six international conferences and eight regional conferences (Appendix B).

He got the best presentation prize awards as shown below

- 1) Best Presentation Award Physical Sciences, Mathematics and Computer Sciences Session: The Science Forum 2011, Faculty of Science, Chulalongkorn University on 11th March 2011
- 2) Best Presentation Award Physical Sciences, Mathematics and Computer Sciences Session: The Science Forum 2013, Faculty of Science, Chulalongkorn University on 15th March 2013
- 3) The First Prize Oral Presentation Award: Siam Physics Congress 2015, Sofitel Krabi Phokeethra Golf and Spa Resort, Krabi, Thailand on 20-22 May 2015

While studying PhD degree, he received financial support from Center of Innovative Nanotechnology (CIN) Chulalongkorn University, The Ratchadaphiseksomphot Endowment Fund of Chulalongkorn University (RES560530227-AM) and The 90th Anniversary of Chulalongkorn University Fund (Ratchadaphiseksomphot Endowment Fund).